Received: 2 June 2022 | Revised: 7 July 2023 | Accepted: 9 July 2023

DOI: 10.1002/gea.21973

RESEARCH ARTICLE

Geoarchaeology An International Journal

WILEY

Geoarchaeological and microstratigraphic view of a Neanderthal settlement at Rambla de Ahíllas in Iberian Range: Abrigo de la Quebrada (Chelva, Valencia, Spain)

M. Mercè Bergadà[1,2] | Aleix Eixea[3] | Valentín Villaverde[3]

[1]Seminari d'Estudis i Recerques Prehistòriques (SERP), Departament d' Història i Arqueologia, Universitat de Barcelona (UB), Barcelona, Spain

[2]Institut d'Arqueologia de la Universitat de Barcelona (IAUB), Barcelona, Spain

[3]Departament de Prehistòria, Arqueologia i Història Antiga, PREMEDOC-GIUV2015-213, Universitat de València, Valencia, Spain

Correspondence
M. Mercè Bergadà, Seminari d'Estudis i Recerques Prehistòriques (SERP), Departament d' Història i Arqueologia, Universitat de Barcelona (UB), C/Montalegre, 6-8.08001 Barcelona, Spain.
Email: bergada@ub.edu

Scientific editing by Sarah Sherwood.

Funding information
Ministerio de Ciencia e Innovación; Generalitat Valenciana

Abstract

The Abrigo de la Quebrada is a Middle Palaeolithic rockshelter located in the Rambla de Ahíllas in the Iberian Range (Valencia, Spain). Archaeological work began in 2007 and was completed in 2015, reaching the rockshelter substratum and uncovering a record that spans from MIS 5 to MIS 4/3. The data from the geoarchaeological and micromorphological study of the site allow us to deduce that it was formed by alluvial contributions from the ephemeral stream, in different subenvironments varying from channel/bar to floodplain facies. These alternate with debris from different displacement processes depending on the unit, such as solifluction–gelifluction, mass displacement, and diffuse runoff. In addition, collapse episodes of the overhanging rockshelter roof influenced the pedological evolution of the record, with implications for the archaeological levels, especially in Unit G (Level IV). From a paleoenvironmental point of view, a more contrasted variability is reflected in the upper units of the site (MIS 4/3), especially in Unit G (Level IV), which, based on data, suggests temperate conditions, and in Unit H (Levels III and II) indicate cold conditions. In contrast, the lower units (MIS 5) are generally temperate, with the exception of Unit C (Level VIIIa), which reflects a colder phase.

KEYWORDS
calcium carbonate features, ephemeral streams, micromorphology, Middle Palaeolithic, palimpsest

1 | INTRODUCTION

The Abrigo de la Quebrada site is located at the contact between the central region in Mediterranean Iberia, near the coast, and the Iberian Range, a medium-altitude mountain range (ca. 1000–2000 m amsl) in the interior of the Iberian Peninsula. Both areas contain Neanderthal occupations (Figure 1a) ranging from MIS 9-8 to MIS 3 (Eixea, Chacón, et al., 2020; Mazo & Alcolea, 2020).

The central Iberian Mediterranean region is an area rich in Middle Palaeolithic sites that are unevenly distributed throughout the territory but tend to be concentrated in the south of the province of Valencia and the north of the province of Alicante. They are linked to different natural corridors: in the north, the Baix Maestrat and the Millars; in the center, the Turia, Magro, and Canal de Navarrés corridors; and in the south, the Vall d'Albaida, Vinalopó, and Vega Baja corridors (Eixea, Chacón, et al., 2020).

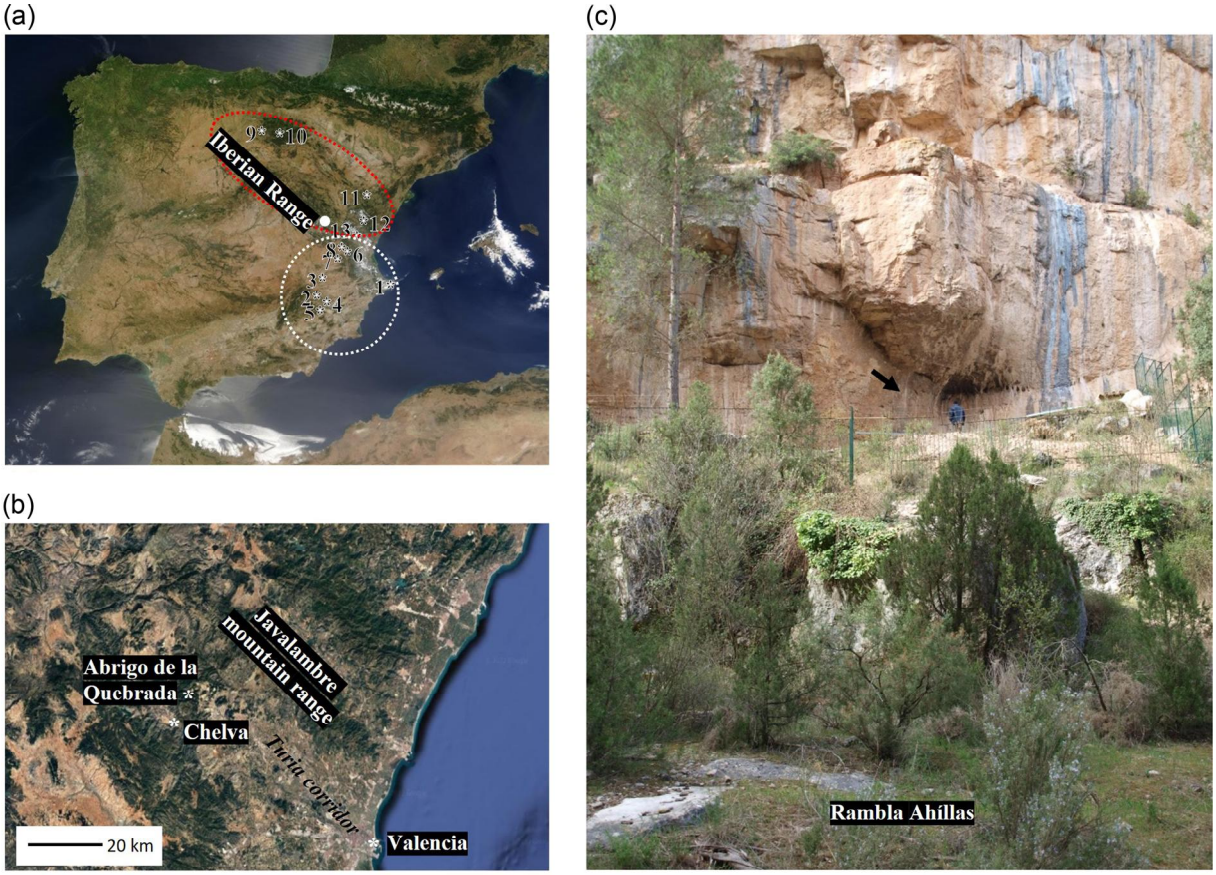

FIGURE 1 Geographical situation. (a) Location of the Middle Palaeolithic sites mentioned in the text. In the white dashed circle, Central Iberian Mediterranean sites: 1. Cova del Bolomor (Valencia); 2. Cova Beneito (Alicante); 3. Cova Negra (Valencia); 4. Abric del Pastor (Alicante); 5. El Salt (Alicante); 6. Rambla de los Morenos (Valencia); 7. San Luís (Valencia); and 8. Abric del Barranc del Carcalín (Valencia). In the red dashed circle, Iberian Range sites: 9. Gran Dolina (Burgos); 10. Peña Miel (Logroño); 11. Los Toros (Teruel); 12. Las Callejuelas (Teruel); and 13. Cuesta de la Bajada (Teruel). The Abrigo de la Quebrada site is marked with a white dot (b). Location of the Abrigo de la Quebrada (Chelva, Valencia). (c) View of the site (marked with a black arrow) from the Rambla de Ahíllas. Drip zones can be observed on the rockshelter wall.

It is in the latter corridor where most of the sites are concentrated, among which the Cova del Bolomor (Fernández-Peris, 2007), Cova Beneito (Doménech, 2005), Cova Negra (Eixea, Oltra, et al., 2020), Abric del Pastor (Connolly et al., 2019), and El Salt (Galván et al., 2014) stand out for their archaeological records. In the central zone, which is the area of interest in our study, there are records such as Rambla de los Morenos, San Luís, and Abric del Barranc del Carcalín (Eixea, Chacón, et al., 2020; Fernández-Peris & Martínez-Valle, 1989), although these sites are not as large as the previous sites mentioned.

In the Iberian Range, archaeological sites located in caves and rockshelters are also numerous and are distributed in two sectors (Mazo & Alcolea, 2020): the northwest, Arlanza basin, in which we highlight some sites such as Gran Dolina (Carbonell et al., 2014) and Peña Miel (Rios-Garaizar & Eixea, 2021; Utrilla et al., 1987), and the southeast, upper Turia basin, the area of interest to us, where the sites of Los Toros (Utrilla & Álvarez, 1985), Las Callejuelas (Domingo et al., 2017), and Cuesta de la Bajada (Santonja et al., 2014), among others, are located.

The site of the Abrigo de la Quebrada, located in the Turia river corridor, specifically in the Rambla de Ahíllas (Figure 1b,c), is an important enclave for information on the Neanderthal populations in this area since it is chronostratigraphically included in MIS 5 and possibly reaches MIS 3 (Carrión-Marco et al., 2019; Eixea, Chacón, et al., 2020; Real et al., 2020). It also has a geogenic and anthropogenic sedimentary record at the base of the rockshelter resting directly on limestone bedrock.

The record offered by the Abrigo de la Quebrada within the regional context is especially important because there are few sites analyzed from a geoarchaeological point of view in alluvial deposits such as the ephemeral streams corresponding to the Middle Palaeolithic, except for the records located in the Altiplano de Yecla in Murcia, Spain (López-Campuzano & Conesa, 2008; López-Campuzano, et al., 2007). These deposits, in general, represent a rare type of record due to the erosive action of the ephemeral streams characterized by steep slopes and a changing morphology. Furthermore, their torrential and sporadic nature does not favor the preservation of lateral deposits and leads to difficulties in

the geomorphological and paleoclimatic interpretation of the site. Our work focuses on analyzing the Abrigo de la Quebrada site from a geoarchaeological point of view, mainly through micromorphological analysis. The specific objectives of our research are to

1. Analyze the variability of the depositional and postdepositional processes involved in the Abrigo de la Quebrada record in detail and clarify the geogenic evolutive history.
2. Distinguish the type of anthropogenic activity recognized in the sedimentary record of the site and resolve if it has been impacted by both depositional and postdepositional geogenic processes. In the latter case, we aim to determine how these processes may have interfered with the preservation of both occupations and archaeological remains.
3. Deduce the paleoenvironmental conditions of the record and its surroundings to better understand the interaction between Neanderthal communities and the environment that they inhabited, and to compare the episodes from MIS 5 with those established during MIS 4/3.

Our geoarchaeological research at the Abrigo de la Quebrada contributes the knowledge of the Middle Palaeolithic occupations in the southeast of the Iberian Range at the beginning of the Late Pleistocene.

2 | THE SITE

2.1 | Location and geological context

The Abrigo de la Quebrada (39°48′25′′N, 01°00′49′′W) is located in Chelva, 69 km northwest of Valencia (see Figure 1b) and 728 m a.s.l. (Badal et al., 2012; Carrión-Marco et al., 2019). Discovered in 2004, and although a test pit was used to evaluate the possibilities of the site, it was not until 2007 that systematic archaeological excavation began (Eixea et al., 2011). This work finished in 2015 after reaching the bedrock of the rockshelter.

The current dimensions of the rockshelter are 38 m wide and between 2 and 9 m deep from the dripline to the back wall, which would have originally extended 11 m. The surface is slightly uneven, with a slight slope in a N–S direction, front to back. Erosional processes on the talus outside the dripline explain the truncation of the record, which would have affected the upper levels of the site. The excavated area was 30 m^2 for the upper levels and about 27 m^2 for the lower levels, with a total thickness of 4 m (Real et al., 2020).

The site is located in the last foothills of the Javalambre mountain range in the Iberian Range (see Figure 1b). The outcropping formations are mainly Middle/Upper Jurassic pisolitic-oolitic limestones and Kimmeridgian micritic limestones, where they alternate in an environment of Lower Jurassic clayey limestones and marls with siltstones and intercalations of Lower Cretaceous Barremian sandstones (Assens et al., 1973; Villaverde et al., 2008).

The Abrigo de la Quebrada is located on the left bank of Rambla de Ahíllas, around 8–10 m above the current river bed. This ephemeral stream, which descends from the Sierra de Javalambre (Pérez-Cueva, 1985), runs through mountainous and steep relief, forming a canyon. In the final stretch, it flows into a plain together with other ephemeral streams, and these feed the river Tuéjar-Chelva, a tributary of the river Turia. At present, Ahíllas is an episodic flood channel, and its water supply is mainly rainwater. Its topographic course generally runs from north to south, although in the study area, it runs from southeast to northwest.

The modeling of this area of Rambla de Ahíllas forms a narrow corridor with an irregular longitudinal profile. Its slopes were formed by steep drops between the tabular limestone strata that shaped the relief of the site, exposing numerous rockshelters (Figure 2a). These are preferentially located in the limestone stratification planes, areas of weakness that favor erosion, as well as by processes of mechanical alteration and dissolution that generated inlets along the limestone in this sector, as is the case of Abrigo de la Quebrada itself. At the foot of the slopes there are mainly boulders and occasional debris.

Thirty meters from the site in a NW direction on the left bank of the ephemeral stream, there are 20–50 cm of alluvial deposits formed by subrounded gravels of mainly micritic limestone with almost no fine-matrix (Figure 2b). Longitudinally furrowed potholes are located in the bedrock and silty–clayey fillings are retained in some sectors. Vegetation colonizing some sectors of the channel (see Figure 2a) is consistent with a river system that alternates flash floods with long periods of water inactivity (Mateo et al., 1988).

The NW orientation of the rockshelter means that direct sunlight is scarce, which is also a consequence of the narrowness of the ravine with its canyon-like characteristics and the steepness of its slopes. Significant drip zones can be observed on the walls of the rockshelter (see Figure 1c), and in some zones, there is an incipient formation of carbonate concretions.

The stratigraphic and sedimentary record of Abrigo de la Quebrada has been obtained mainly from the archaeological profiles shown in Figure 3a,b. The description of the lithostratigraphic units, from bottom to top, is presented in Table 1 and Figure 3c. Some features of the field description of units C, D, and E are reflected in Figures 4 and 5.

2.2 | Archaeological assemblage

The Abrigo de la Quebrada comprises nine archaeological levels. Human presence corresponding to the Middle Palaeolithic is recorded in throughout the site, except Levels I and VI. Level I corresponds mostly to the use of the rockshelter as a stable in historical times and will not be dealt with in this article. For Level VI, two optically stimulated luminescence dates on the feldspar fraction are 80,000 ± 4700 a and 83,200 ± 5400 a (Carrión-Marco et al., 2019; Real et al., 2020).

From an archaeological point of view, the levels ranging from II to V contain the most evidence of occupation and have several radiocarbon dates. Levels III–V were dated by radiocarbon

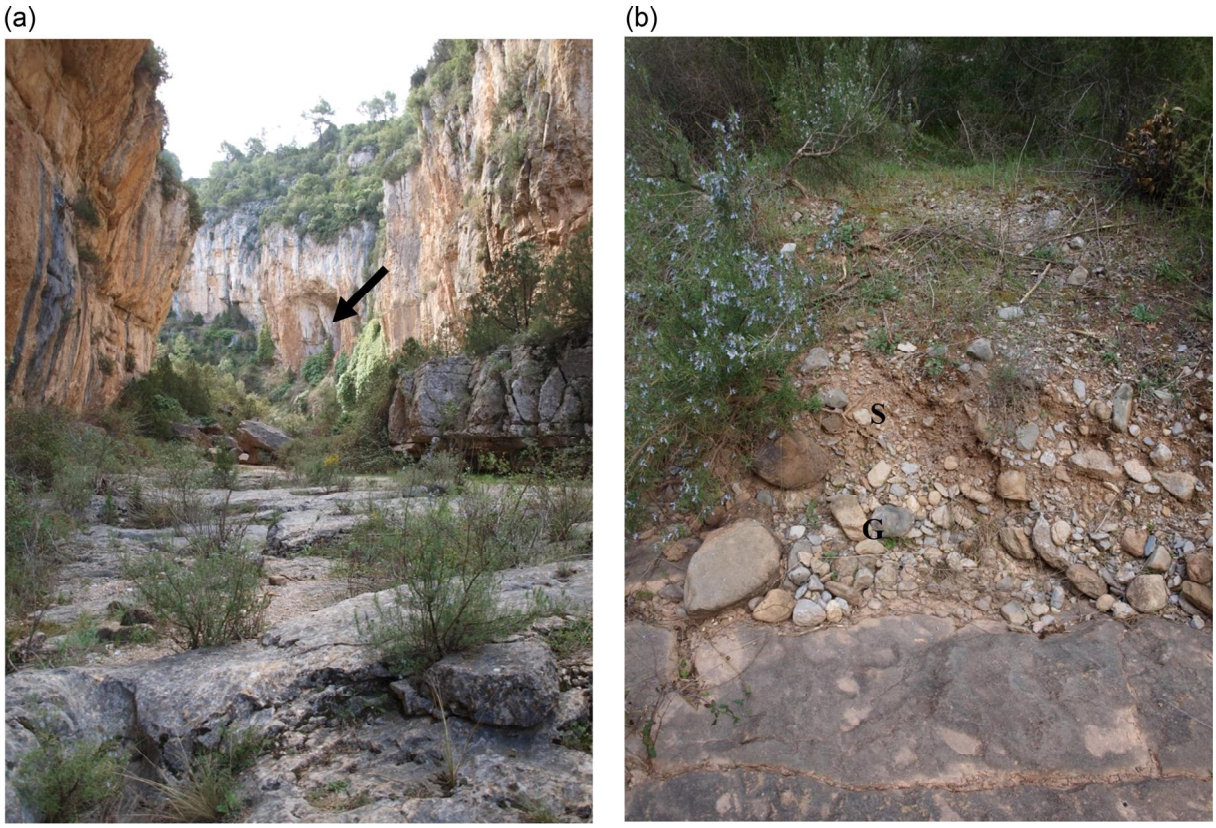

FIGURE 2 Views of the Rambla de Ahíllas. (a) General view of the canyon, showing the formation of rockshelters (black arrow), as well as the colonization of vegetation in some parts of the river bed. (b) Fluvial sedimentary sequence of the Rambla de Ahíllas near Quebrada showing rounded to subrounded gravels (G), overlain by an increase in sand (S).

accelerator mass spectrometry: III at 40,500 ± 530 14C a B.P. and IV at 43,930 ± 750 14C a B.P. (Real et al., 2020; Villaverde et al., 2008), although Levels III and IV were also dated by acid–base oxidation, giving results >50,800 14C a B.P. and >51,600 14C a B.P. (Eixea et al., 2011–2012) and V > 47,100 14C a B.P. (Real et al., 2020). The lithic industry includes discoid and centripetal Levallois technologies, and the tools are simple sidescrapers and Mousterian points. The abundance of cortical fragments, cores, and flakes of different sizes suggests that the knapping was carried out in situ (Carrión-Marco et al., 2019). Flint, mainly local, was used as raw material, although other raw materials are also used like limestone and quartzite (Eixea, Chacón, et al., 2020). In the fauna, mainly from Level IV, remains of eight different families were identified: Bovidae, Equidae, Cervidae, Leporidae, Testudinidae, Suidae, Rhinocerotidae, and Canidae. Ibex (*Capra* sp.), horse (*Equus ferus*), and deer (*Cervus elaphus*) are the most abundant taxa (Carrión-Marco et al., 2019; Real et al., 2020). With regard to the microfauna, *Microtus cabrerae* has been detected in Levels II and V (Carrión-Marco et al., 2019).

The lower levels of the record, from VII to IX, have not been absolutely dated and present a different pattern of lithic and faunal remains, especially in Levels VII and VIII (Eixea, Chacón, et al., 2020; Villaverde et al., 2017). In the lithic industry, discoid knapping dominates and the raw material is mainly flint. Regarding the fauna, specifically in VII, leporids are the best represented group and are likely the result of nonanthropic consumption activities. The leporids are followed by ungulates, with the *Equidae* families standing out, of which part of the sample could correspond to the donkey (*Equus hydruntinus*), followed by Cervidae and Bovidae–Caprinae, most of which seem to correspond to activities of Neanderthal groups (Real et al., 2019). Microfauna of Levels VII and VIII include *Arvicola sapidus*, *Microtus cabrerae*, *Terricola duodecimcostatus*, and *Apodemus* sp., with *Elyomis quercinus* present only in VIII (Carrión-Marco et al., 2019).

The archaeobotanical data from the excavations show the same anthracological taxa at all levels, such as *Ephedra* sp. (joint pine), Ericaceae (heather), *Juniperus* sp. (juniper), monocotyledons, *Pinus nigra* and/or *P. sylvestris* (black and/or Scots pines), *Pinus* tp. *pinaster* (maritime pine), *Pinus* sp., cf. *Pistacia* sp., evergreen *Quercus* sp. (holm oak, kermes oak), *Quercus* sp., cf. *Rosmarinus officinalis* (rosemary), and *Viburnum* sp. Carpological remains of *Celtis*, of possible Fabaceae, and other angiosperms were also identified. Level VIII has the highest taxonomic diversity and III has the lowest. In general, pines dominate (80%–90%) and angiosperms (5%–10%) are the least prevalent (Carrión-Marco et al., 2019). The phytolith analyses focus especially on the upper levels, from which it can be deduced that herbaceous plants

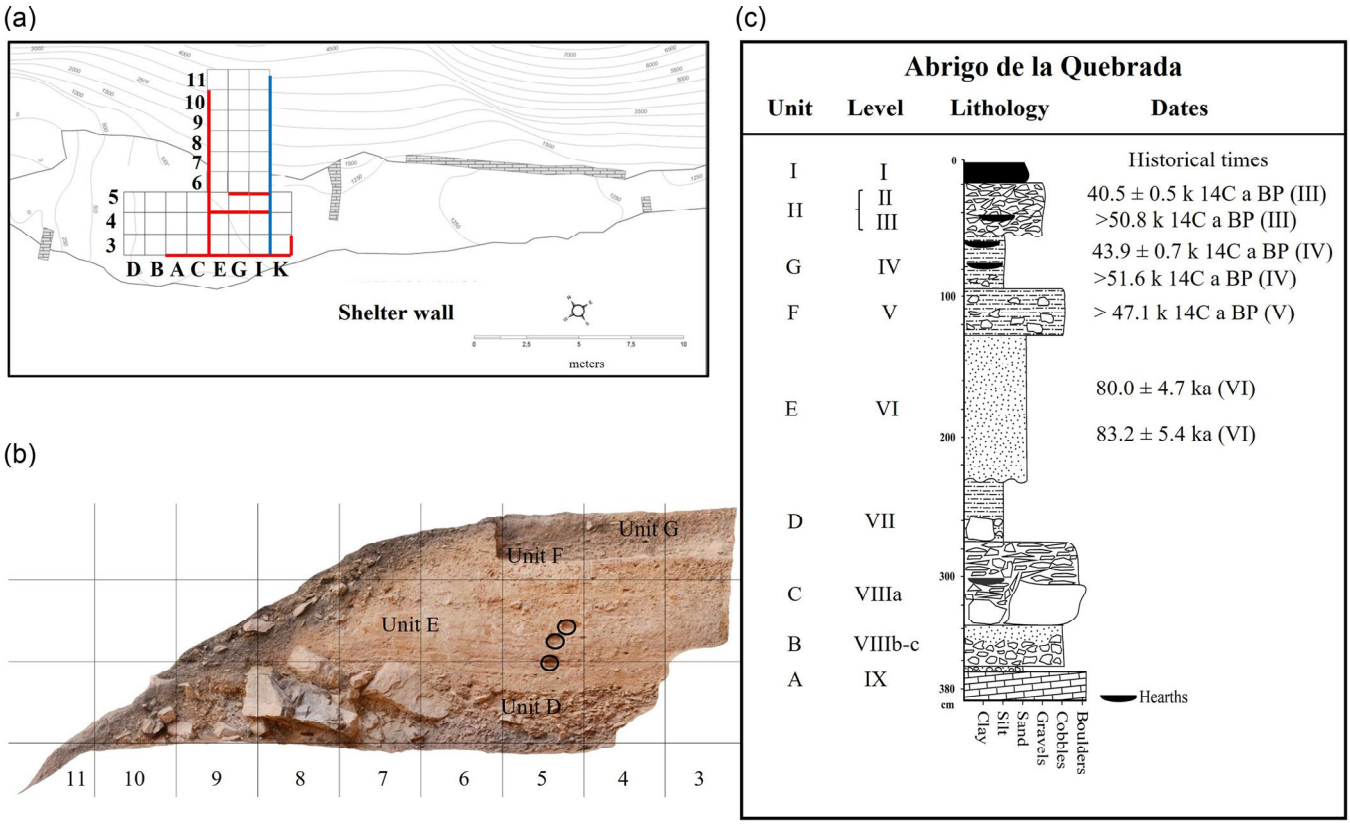

FIGURE 3 Location of the main sectors studied. (a) Plan of the site, showing the sections analyzed in red and in blue, situation of the profile image in (b). (b) Right sagittal profile, seen from bottom to top: Unit D (AL VII) with blocks, the central part of Unit E (AL VI) and the upper part of Unit F (AL V) and part of Unit G (AL IV). The OSL sampling of Unit E is circled. (c) Stratigraphic column of Abrigo de la Quebrada showing the different lithostratigraphic units, archaeological levels, and dates. AL, archaeological level; OSL, optically stimulated luminescence.

dominate, although leaves and wood/bark of woody plants are also found (Esteban et al., 2017).

The available paleoecological and technological data suggest that the Neanderthal communities that inhabited the site exploited the immediate environment by hunting ibex, horse, and deer in a pine forest environment. Most of the lithic raw material corresponds to local flint and comes from an area within 2–8 km (Eixea et al., 2011).

3 | METHODS

The study procedure that we used consisted of stratigraphic–sedimentary field description (see Table 1) and the application of soil micromorphology applied to the entire stratigraphic record, except for Unit B, in which we were only able to sample the sandy laminations. The study was based on the following profiles of the site's grid: A-3, C-3, E/3-4, E-4, E-5, E-7, G-5, I-4, I-5, I/4-5, and K-3 (Figure 6a–f). The analysis of some combustion areas, specifically in profiles E-3 and I-5, and grid square G-3 is also included in the study.

The protocol that we followed for the extraction of intact block samples, a total of 20, consisted of introducing the sediment into boxes covered with plaster, which allowed us to obtain blocks without altering the structure and arrangement of the sediments. Samples collected by M. Mercè Bergadà were processed at the Micromorphology and Image Analysis Service in the Department of Environmental and Soil Sciences at the University of Lleida. The blocks were air-dried and then oven-dried at 40°C for 48 h to minimize precipitation of soluble salts during sample drying. They were then impregnated with an unsaturated colorless orthophthalic polyester resin and diluted with styrene at a ratio of three parts resin to one part styrene with a Methyl Ethyl Ketone Peroxide catalyst and activator (cobalt octoate). The embedded blocks were cut into smaller blocks a few centimeters thick and two thin sections were made for each block, generally 13.5 × 5.5 cm in size, although some are 7.7 × 5.5 cm and all are 30 µm thick. Thin sections (in total 43) were observed under a polarizing stereomicroscope and a petrographic microscope at magnifications between ×6.3 and ×400, using plane-polarized light (PPL), crossed-polarized light (XPL), and oblique incident light (OIL). Thin-section description and interpretations follow the guidelines proposed by Bullock et al. (1985), Stoops (2021), Stoops et al. (2010), and Nicosia and Stoops (2017).

When presenting the microstratigraphic study of the stratigraphic units, we use the term microunit (MU) to distinguish

TABLE 1 Stratigraphic and sedimentary field description of Abrigo de la Quebrada.

Profiles	Unit (AL)	Thickness	Color	Field description	Period	Dates
I/4-5	A (IX)	5.5 cm	7.5YR7/2	*Sands with cobbles and pebbles with $CaCO_3$*: It is made up of light brown sands with cobbles and subrounded limestone pebbles and is fully cemented. It is in contact with the limestone substrate of the rockshelter.	Middle Palaeolithic (some industrial and bone evidence)	
I/4-6	B (VIIIb and c)	26 cm	7.5YR5/4	*Angular gravels and sandy laminations*: Composed of some thin intercalations of angular gravels, in the form of platelets <6 cm with slight concretions toward the lower part, with some laminations of fine and medium brown sands. In profile I/6, there is a net contact with respect to the previous unit.	Middle Palaeolithic (an increase in archaeological material)	
I/3-5 E/3-6 G/3-5	C (VIIIa)	35–60 cm	7.5YR6/2	*Clasts and boulders*: Slopes toward the north northeast. It consists of a deposit of platy clasts <15 cm with grayish-brown sandy silts with practically no carbonate concretions, except for profile E-6. In profile E-4, the platy clasts, 12–15 cm, appear in a vertical arrangement together with some blocks. The clasts deposit is located in sector E-G-I/3-5, totaling 9 m^2, and the blocks make up the rest of the excavated area. There are combustion features, specifically the one located in the profile E-3, about 12 cm in length with a thickness of 5 cm, that could be described and is distinguished by a whitish calcitic accumulation (7.5YR6/1) next to charcoal.	Middle Palaeolithic	
E/4-7 G-I/4	D (VII)	43 cm	7.5YR6/4	*Silty clays with cobbles and some boulders*: Composed of brown silty clays with subangular to subrounded limestone cobbles, and some are carbonate fragments. Toward the base of the unit, there are blocks with traces of carbonation and toward the top, they decrease in size and the presence of cobbles increases. The E-G-I/4 sector is where its geometry is best represented, with a tabular tendency and a slight northeast slope. Toward the top, there are traces of biological activity (roots and soil fauna activity). Diffuse contact in sectors close to the wall of the rockshelter and abrupt toward Rambla de Ahillas.	Middle Palaeolithic	
E/3-7 C-3 G-I/4 I/3-7	E (VI)	90–100 cm	7.5YR5/6	*Sands*: Sands with brown silty–clay laminations with some scattered gravels, especially in C/E-3, the inner sector of the rockshelter, with some $CaCO_3$ nodules. The contact is erosive and has a wavy bedding, especially in profile G-I/4.	Sterile	80.0 ± 4.7 ka and 83.2 ± 5.4 ka
A-3 C-3 K-3	F (V)	33 cm	7.5YR6/4-7.5YR5/2	*Cobbles with silty clays*: Formed by subangular limestone cobbles and gravels oriented in the direction of the slope with a north northwest tendency and with some overlapping, especially in the K-3 grid square. At the base and especially in the A-3 and K-3 grid-squares, there are blocks and cementation is visible in the deposit, and toward the top, the size of the gravels	Middle Palaeolithic	>47.1k 14C a B.P.

TABLE 1 (Continued)

Profiles	Unit (AL)	Thickness	Color	Field description	Period	Dates
				decreases. The matrix is made up of silty clays with brown sands, although toward the top, they are darker in color and the clay fraction increases significantly. Geometry with a tabular tendency and diffuse contact with respect to the E episode, especially in the sector of the rockshelter wall.		
C-3 K-3 I/4-5 G/3-5 E-5	G (IV)	20–40 cm	7.5YR5/4	*Silty clays*: Formed by silty clays with brown-colored sands and with subangular cobbles and gravels that diminish toward the outside of the rockshelter. Cementation can be seen in some sectors, as well as an increase in organic matter. Archaeological components and combustion areas abound. Very diffuse contact and the geometry tends to be tabular.	Middle Palaeolithic	43.9 ± 0.7k 14 C a B.P. and >51.6k 14C a B.P.
A/3-5 E-5 G-I-K/5	H (III-II)	37 cm	7.5YR6/4- 7.5YR5/4	*Gravels with sandy silt*: Characterized by angular and subangular gravels giving rise to 1–4 cm platy clasts limestone that tend to decrease toward the G-I-K/5 sector and with a subrounded morphology. Toward the top, they appear with $CaCO_3$ concretions, especially in grid square A-3, and the sandy silt matrix is brown. Erosive contact in some sectors, especially in those between A/3-5, and its geometry tends to be irregular. There are combustion features, specifically a flat combustion area in profile I-5, where the following sequence from bottom to top was distinguished: 2. Thickness <1 cm consisting of a dark brown silty–clay fraction (7.5YR5/4) with charcoal residues. 1. Thickness 1.7 cm. Composed of whitish calcitic accumulation (2.5YR7/2), with some silty sands and some limestone gravels.	Middle Palaeolithic	40.5 ± 0.5k 14C a B.P. and >50.8k 14C a B.P. (III)
A-3	I (I)	5–11 cm	7.5YR5/0	*Organic material*: Silty sands with subrounded gravels and organic residues, with a tabular geometry and a net contact.	Historic period	

Abbreviation: AL, archaeological level.

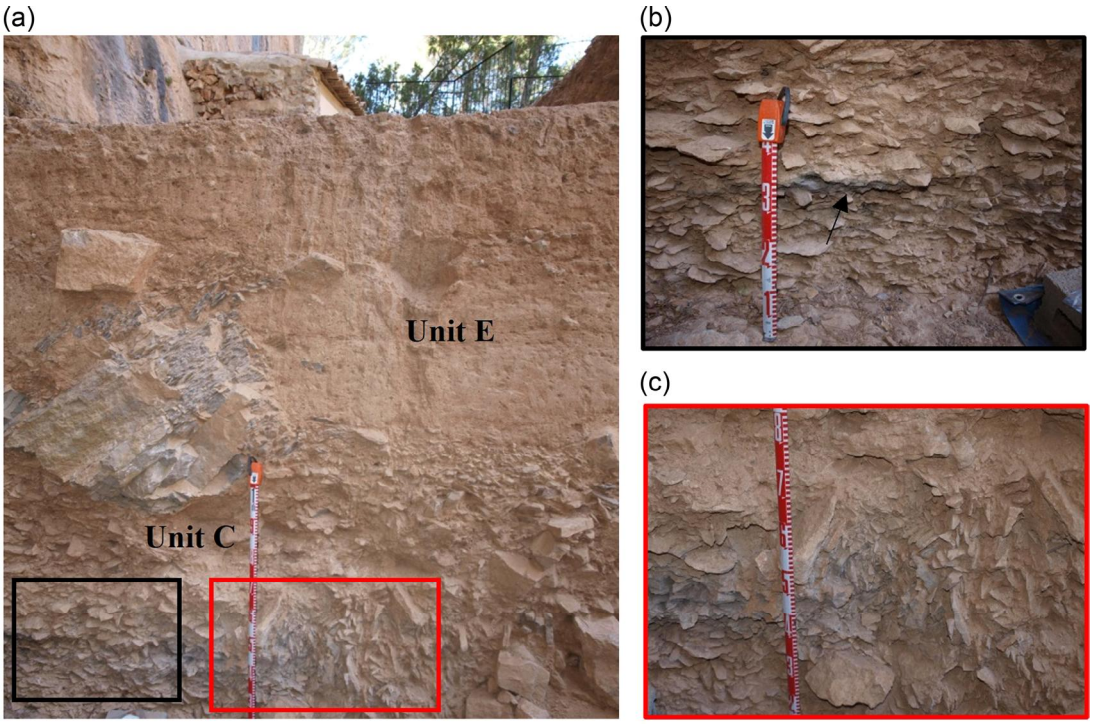

FIGURE 4 Profile E/3-4. (a) General view, showing Unit C (AL VIIIa) and Unit E (AL VI) location of image (b)—black, image (c)—red. (b) Detail of the arrangement of the horizontal platy clasts; note the ashy residues. The sampling area of Sample 12 is indicated by the arrow. (c) Clasts in vertical arrangement also due to the presence of blocks that restricted deposition. AL, archaeological level.

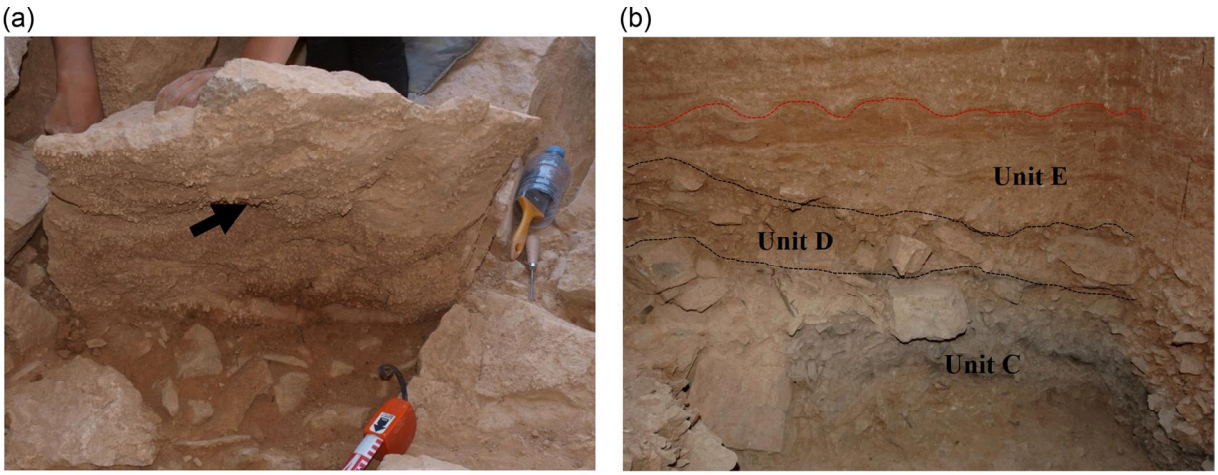

FIGURE 5 Detail of Units D and E. (a) Unit D (AL VII). General view of a block in a vertical position showing the formation of carbonate concretions (black, arrow). (b) Units C (AL VIIIa), D (AL VII), and the basal part of Unit E (AL VI), shown in the G-I/4 profile. The wavy bedding is shown in red. AL, archaeological level.

microstratigraphic units identified in thin section. In the case of the record analyzed, some of the MU coincide with the field units and their facies, and only in some cases microscopic observation has been able to detail additional MU (Table 2). We included the micromorphological analysis of the combustion areas in each unit to better contextualize the anthropogenic activity.

4 | RESULTS

In this section, we present the most important micromorphological aspects of each unit and MU in stratigraphic order. These are shown in more detail in Table 3. From now on, when we refer to archaeological levels, they will be referred to with the acronym AL.

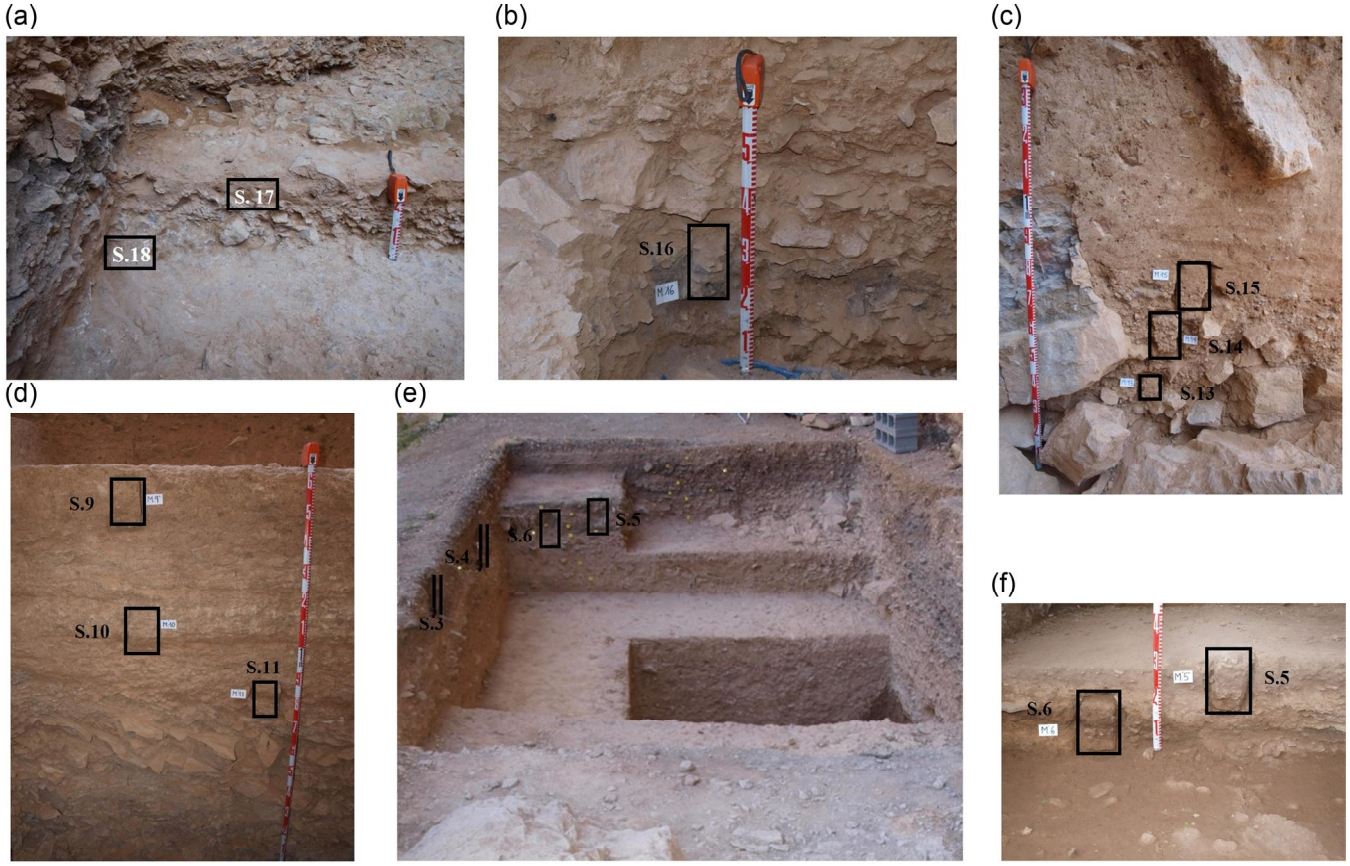

FIGURE 6 Detail of micromorphological sampling. (a) Profile I/4-5: S.18 (Unit A, AL IX) and S.17 (Unit B, AL VIIIb-c). (b) Profile I-5: S.16 (Unit C, AL VIIIa). (c) Profile E-7: S.13 and S.14 (Unit D, AL VII) and S.15 (Unit D, AL VII–Unit E, AL VI). (d) Profile E-4: S.11, S.10 and S.9 (Unit E, AL VI). (e) Profile E-G/5 marking the following samples: S.3 (Unit G, AL IV–Unit H, AL III-II) and S.4 (Unit G, AL IV) and Profile I-5: S.5 (Unit G, AL IV–Unit H, AL III-II) and S.6 (Unit G, AL IV). (f) Detail of profile I-5. Samples 5 and 6. The upper part of S.5 includes the Unit H hearth. AL, archaeological level.

The descriptions are complemented by the interpretations presented in the *Discussion* section. Micromorphological characteristics such as the composition of the coarse fraction and the micromass are generally the most homogeneous features of the record and are highlighted as follows:

The lithological and mineralogical composition consists mainly of limestone (pisolithic, oolitic, and micritic), mostly subangular to subrounded, as well as quartz, feldspar, and calcite. Muscovite and glauconite also occur in Units A, B, and E. Anthropogenic components are common, except in Unit E and to a lesser extent in Units A and B, with the majority in Unit G. Biogenics components such as bones and teeth with various traces of thermoalteration are present. Particularly noteworthy are fat-derived char in Units D and G, terrestrial molluscs, especially in Unit D, and some coprolites in Unit G. Charred fragments such as charcoals and plant remains are common and predominate in Units F and G. Calcitic ashes appear in Units C, G, and H. Silica phytoliths are also found in Units C, D, F, G, and H. The micromass is mainly calcitic crystallitic, although in some units, it also appears as an undifferentiated type, in the case of Unit C, as phosphatized clayey, and in others due to the increase of amorphous organic matter, especially in Unit G. The other micromorphological features described vary between units and MU.

4.1 | Microstratigraphic description

The units and MU analyzed are as follows (see Table 3):

Unit A (AL IX) is represented by MU.1. Poorly sorted coarse and medium sands dominate, with subrounded pebbles and cobbles of pisolithic-oolitic and micritic limestone (Figure 7a). It is matrix-supported and occasionally clast-supported. There are some reworked bones and subangular flint fragments in the basal part. The carbonate groundmass with microsparite crystallization (Figure 7b) and with traces of calcitic depletion in some zones, as well as calcitic coatings mainly in sands (Figure 7c) appear as pedofeatures. Unit B (AL VIIIb and VIIIc) is only represented in thin section by MU.2. It is composed of fine and medium subrounded sands with some rounded pebbles and cobbles, the same lithology as Unit A. There are also some woody charcoal fragments and bones of a larger size than the sand fraction. The calcitic hypocoatings in vughy voids, sometimes together with fine material and hypocoatings of Fe oxides and hydroxides, stand out as pedofeatures.

Unit C (AL VIIIa) is represented by the MU.3 and is characterized by the presence of subangular clast-supported pisolithic-oolitic limestone fragments (see Figure 4b). Some show in situ cracking

TABLE 2 Correlation of the units and microunits of Abrigo de la Quebrada.

Units (AL)	Main stratigraphic features	MU	Main microstratigraphic features
A (IX)	Sands with cobbles and pebbles with $CaCO_3$	MU.1	Coarse-medium sands and pebbles with $CaCO_3$.
B (VIIIb-VIIIc)	Angular gravels and sandy laminations	MU.2	Fine and medium sands.
C (VIIIa)	Clasts and boulders	MU.3	Platy clasts.
D (VII)	Silty clays with cobbles and some boulders	MU.4	Silty clays and gravels.
E (VI)	Sands	MU.5	Ungraded sands.
		MU.6	Ungraded sands.
		MU.7	Well-sorted fine/medium sands.
		MU.8	Well-sorted coarse sands.
		MU.9	Well-sorted fine/medium sands (clay aggregates).
		MU.10	Well-sorted fine/medium sands.
		MU.11	Well-sorted fine/medium sands (clay aggregates).
		MU.12	Well-sorted fine/medium sands.
		MU.13	Well-sorted coarse sands.
		MU.14	Well-sorted fine/medium sands (clay aggregates).
		MU.15	Clayey silts.
		MU.16	Clayey silts.
		MU.17	Clayey silts.
		MU.18	Clayey silts.
F (V)	Cobbles with silty clays	MU.19	Gravels with silty clays with $CaCO_3$.
		MU.20	Silty clays with organic and charcoal residues.
G (IV)	Silty clays	MU.21	Silty clays with $CaCO_3$.
		MU.22	Silty clays with organic and charcoal residues.
		MU.23	Silty clays with $CaCO_3$.
		MU.24	Silty clays with organic and charcoal residues.
H (III-II)	Gravels with sandy silt	MU.25	Gravels with silty sands.
		MU.26	Silty sandy gravels with silt capping.

Abbreviations: AL, archaeological level; MU, microunit.

(Figure 8a,b), and some fragments also appear in a vertical position, especially in profile E/3-4, in particular, Sample 12a. The micromass is yellowish brown of clay and silty fine material, slightly undifferentiated b-fabric (Figure 8c,d), with a channel microstructure and vesicular voids in some zones. Compared to the previous MU, there is an increase in woody charcoal, some with traces of fragmentation, as well as bone remains and some tooth fragments. In some areas, especially in grid square I-5 (Sample 16), laminar crusts of calcium carbonate with spherulites of about 100 μm (Figure 8e,f) and traces of dissolution appear as pedofeatures. Calcitic pendants are also found below gravels and are composed of successive laminae ranging from clear, micritic to dark brown, dominated by detrital material. Finally, we highlight the coatings and hypocoatings of fine material, clays, with oriented domains, especially in profile E/3-4 (Sample 12a). In the combustion area located in profile E-3 (see Figures 4b and 9a,b), there is a 6.5-mm-thick calcitic accumulation with some prismatic calcium carbonate pseudomorphs and ashes (Figure 9c). In the lower part, there are light impregnations of Fe oxides and hydroxides with some charcoal residues (Figure 9d). Pedofeatures include coatings and hypocoatings of fine material with oriented domains (see Figure 9c), and the detrital material appears with traces of brunification and impregnations of Fe oxides and hydroxides.

Unit D (AL VII) is represented by MU.4, which is characterized by the presence of carbonate concretions in the gravels and carbonate fragments. Some of these concretions appear with banded laminations, some micritic and lighter in color, and some detrital and darker (Figure 10a); others also appear with microcrystalline, laminated fabric and with a palisade or columnar habit in which the growth points of the crystals can be seen (Figure 10b,c) (J. M. Cervelló,

TABLE 3 Main micromorphological characteristics of the Abrigo de la Quebrada.

Unit (AL) Sample, profile	Microunits	Microstucture	Groundmass	C/f rel.dist. pattern	Coarse material			Micromass	Pedofeatures
					Rock fragments	Minerals	Organic and inorganic fragments		
A (IX) S.18, I/4-5	MU.1. Coarse medium sands and pebbles with $CaCO_3$	Vughy/vesicular. 10% porosity.	c/f 50 μm 3/1	Close porphyric	Micritic (***) and pisolithic-oolitic (***) limestone (SR/R).	Quartz (*****) and feldspar (**) (SA-SR), muscovite (*), calcite (**).	Bone fr. and flint.	Calcitic crystallitic b-fabric.	$CaCO_3$ crust and infillings of the microsparite crystallization (+++++), traces of calcitic depletion (+++), calcitic coatings in sands (++), orthic nodules of Fe (hydr) oxides (+).
B (VIIIb-VIIIc) S.17, I/4-5	MU.2. Fine and medium sands	Vughy/granular. 15% porosity.	c/f 50 μm 3/1	Gefuric/close porphyric	Micritic (***) and pisolithic-oolitic (***) limestone (SR/R).	Quartz (*****) and feldspar (**) (SR/SA), calcite (**), glauconite (*), muscovite (*).	Charcoal fr. (*), bone fr. (*).	Calcitic crystallitic b-fabric.	Calcitics and fine material hypocoatings (++), calcium carbonate infillings (+), coatings of fine material in voids, Fe(hydr)oxides hypo-coatings (++), orthic nodules of Fe (hydr)oxides (+).
C (VIIIa) S.16, I-5 and S.12a, E/3-4	MU.3. Platy clasts	Channel and granular. 20% porosity. Some vesicles.	c/f 50 μm 3/1	Single-spaced porphyric	Pisolithic-oolitic (*****) limestone (A-SA), slight fragmentation in situ, some appear in a vertical arrangement.	Quartz and feldspar (A) (**) and calcite.	Charcoal fr. (***), silica phytoliths (S.12. ***), some gastropod fr., spherulites (**), bones, and tooth fragments (***) with combustion traces.	Yellowish brown (PPL) clays, undifferentiate-d/calcitic crystallitic b-fabric.	$CaCO_3$ laminar crust (++++) in S.16; pendants in gravels (+++), calcitic hypocoatings (++), clay hypocoatings and coatings (++++), especially in S.12a.
D (VII) S.13, 14 and bottom 15, E-7	MU.4. Silty clays and gravels	Channel/ granular. 25% porosity. Some vesicles.	c/f 50 μm 1/2	Double-spaced porphyric	Pisolithic-oolitic limestone and carbonate fragments (*****) (SA).	Quartz and feldspar (A) (**) and calcite.	Gastropods (***), silica phytoliths (**), spores (*), fat-char (*), charcoal fr. (*), bone fr. (*).	Brown (PPL) clays, calcitic crystallitic b-fabric.	Dissolution traces (+), pendant calcitic (++), hypocoatings in voids (+++), dense incomplete phytomorphic calcite infillings (++), biogenic calcite granules(+).
E (VI) S.15, E-7	MU.5. Ungraded sands (5 cm thick)	Single grain. 15% porosity.	c/f 50 μm 3/1	Single-spaced porphyric/ chitonic	Pisolithic-oolitic (***) and micritic (**) limestone (SA).	Quartz and feldspar (***) (SA-SR) and calcite.		Calcitic crystallitic b-fabric.	Traces of dissolution on the cobbles (+), calcitic hypocoatings in cobbles (+), loose discontinuous infilling of acicular calcite (+).

(Continues)

TABLE 3 (Continued)

Unit (AL) Sample, profile	Microunits	Microstucture	Groundmass	C/f rel.dist. pattern	Coarse material			Micromass	Pedofeatures
					Rock fragments	Minerals	Organic and inorganic fragments		
E (VI) S.15, E-7	MU.6. Ungraded sands (7 cm thick)	Single grain. 15% porosity.	c/f 50 μm 2/1	Single-spaced porphyric/ chitonic	Pisolithic-oolitic limestone (**) (SA) and red clay aggregates (**).	Quartz and feldspar (****) (SA-SR).		Brown (PPL) silty clays, calcitic crystallitic b-fabric.	Concentric orthic nodules of Fe (hydr)oxides (++).
E (VI) S.11, E-4	MU.7. Well-sorted fine/ medium sands (3 cm thick)	Pellicular grain/ granular. 15% porosity.	c/f 50 μm 3/1	Single-spaced porphyric/ single-spaced fine enaulic	Micritic limestone (*) (SR) and red clay aggregates (*).	Quartz and feldspar (****) (SA-SR) and muscovite (*).		Calcitic crystallitic b-fabric.	Clay hypocoatings in voids (+).
E (VI) S.11, E-4	MU.8 (1.5 cm) and MU.13 (3.3 mm). Well-sorted coarse sands	Pellicular grain/ massive. 15% porosity.	c/f 50 μm 3/1	Coarse monic	Micritic limestones (SR-R)**, clay aggregates (**).	Quartz and feldspar (***) (SR) and muscovite.	Some charcoal fr. (MU.13).	Calcitic crystallitic b-fabric.	Clay hypocoatings in voids (+) and anorthic calcite nodules (++).
E (VI) S.11, E-4	MU.9 (3.5 cm), MU.11 (1.4 cm) and MU.14 (7 mm) (S.11). Well-sorted fine/ medium sands (clay aggregates)	Pellicular grain/ massive. 5%–15% porosity.	c/f 50 μm 3/1	Coarse monic/ close porphyric	Some micritic limestones (SR-R), clay aggregates (**).	Quartz and feldspars (****) (SR), chert (MU.14) and muscovite.		Brown-red (PPL) clays, calcitic crystallitic b-fabric.	Anorthic nodules of Fe (hydr)oxides (+), clay hypocoatings in voids (+) and anorthic calcite nodules (+).
E (VI) S.11, E-4	MU.10 and MU.12 (5–7 mm thick) (S.11). Well-sorted fine/ medium sands	Pellicular grain/ massive (MU.12). 5%–10% porosity.	c/f 50 μm 3/1	Chitonic/close porphyric	Some micritic limestones (SR-R)(*).	Quartz and feldspar (****) (SA-SR) and muscovite.		Calcitic crystallitic b-fabric.	Calcite hypocoatings in voids (+).
E (VI) S.10, E-4	MU.15. Clayey silts (2.5 cm thick)	Pellicular grain/ massive. 25% porosity.	c/f 50 μm 3/1	Chitonic/monic	Micritic limestone (**) (SR-R), clay aggregates (*).	Quartz and feldspars (****) (SR), chert, and muscovite.		Brown (PPL) clays, calcitic crystallitic b-fabric.	Clay infillings (+), clay hypocoatings (+), anorthic calcite nodules (+).
E (VI) S.10, E-4	MU.16. Clayey silts (2.5 cm thick)	Intergrain microag-gregate. 20% porosity.	c/f 50 μm 2/1	Enaulic	Micritic limestone (*) (SR-R).	Quartz and feldspar (***) (SA).	Some charcoal fr.	Brown (PPL) clays, calcitic crystallitic b-fabric.	Biogenic calcite granules (++), clay hypocoatings (++), anorthic calcite nodules (+).

TABLE 3 (Continued)

Unit (AL) Sample, profile	Microunits	Microstucture	Groundmass	C/f rel.dist. pattern	Coarse material			Micromass	Pedofeatures
					Rock fragments	Minerals	Organic and inorganic fragments		
E (VI) S.10, E-4	MU.17. Clayey silts (7 cm thick)	Channel. 10% porosity.	c/f 50 μm 1/3	Double-spaced porphyric	Some pisolithic-oolitic and micritic limestone (SR-R).	Quartz and feldspar (**) (SA), muscovite.	Some charcoal fr.	Brown (PPL) clays, calcitic crystallitic b-fabric.	$CaCO_3$ crust and infillings (++), biogenic calcite granules (++), clay hypocoatings (++), anorthic calcite nodules (+).
E (VI) S.9, E-4	MU.18. Clayey silts (13 cm thick)	Vughy. 15%–20% porosity.	c/f 50 μm 2/1	Single-spaced porphyric/ gefuric	Micritic and pisolithic - oolitic limestone (*) (SR).	Quartz and feldspar (**) (SA).		Brown (PPL) clays, calcitic crystallitic b-fabric.	Calcitic hypocoatings (++), fecal pellets, and passage features (++).
F (V) S.8, K-3	MU.19. Gravels with silty clays with $CaCO_3$	Vughy/vesicular. 15% porosity.	c/f 50 μm 2/1	Single-spaced porphyric	Pisolithic-oolitic limestone (***) (SR-SA).	Quartz and feldspar (**) (SA).	Silica phytoliths (*), charcoal fr. (**), bone fr. (***), malacological fr. (*), flint fr. (*), tooth fr. (*).	Brown (PPL) clays, calcitic crystallitic b-fabric.	$CaCO_3$ infillings (dense incomplete/loose discontinuous), traces of calcitic depletion (+), calcitic coatings in gravels (++) granular bioaggregates (++).
F (V) S.7, C-3	MU.20. Silty clays with organic and charcoal residues	Granular/ crumbly. 25%–30% porosity (channels and vughy).	c/f 50 μm 1/2	Single-spaced porphyric	Pisolithic-oolitic and micritic limestone (***) (SR-SA).	Quartz and feldspar (**) (SA) and calcite.	Silica phytoliths (**), AOM (**), charcoal fr. (**), bone fr. with thermoalteration traces (****), flint fr. (*).	Brown (PPL) clays, calcitic crystallitic b-fabric.	$CaCO_3$ coatings in bones (+++), calcitic hypocoatings, silty–clay coatings in gravels (++), dense incomplete infillings of phytomorphic calcite, queras (++), loose discontinuous infillings of acicular, granular bioaggregates (++).
G (IV) S.6, I-5; S.4, G-5; S.19, G-3; S.20, I-4	MU.21. (Bottom S.6 and bottom S.4) and MU.23 (top S.6, S.19 and S.20). Silty clays with $CaCO_3$.	Vughy and channel/ massive. 20% porosity.	c/f 50 μm 2/1	Close porphyric	Pisolithic-oolitic limestone (*) (SR) MU.21 thermoalteration cracks.	Quartz and feldspar (**) (SA) and calcite.	Charcoal fr.(**), ash fr. (*) bone fr. with thermoalteration traces (***), malacological fr. (*) flint fr. (*).	Brown (PPL) clays, calcitic crystallitic b-fabric.	$CaCO_3$ impregnations in the groundmass (++++), dense incomplete infillings of phytomorphic calcite, queras, coatings, and hypocoatings in bones (+++), yellow cryptocrystalline hypocoatings in the detrital material (+) ellipsoidal fecal pellets (+++).

(Continues)

TABLE 3 (Continued)

Unit (AL) Sample, profile	Microunits	Microstucture	Groundmass	C/f rel.dist. pattern	Coarse material			Micromass	Pedofeatures
					Rock fragments	Minerals	Organic and inorganic fragments		
G (IV) S.6, I-5; S.4, G-5; S.5, I-5; S.3, E-5	MU.22. (Middle S.6 and top S.4) and MU.24 (bottom S.3 and bottom S.5). Silty clays with organic and charcoal residues.	Granular and crumbly. 10%–20% porosity.	c/f 50 μm 1/2	Double-spaced porphyric	Pisolithic-oolitic limestone (*) (SR) with dissolution traces, thermoalteration cracks (MU.22).	Quartz and feldspar (**) (SA) and calcite.	Charcoal fr. (***), ash fr., AOM (***), silica phytoliths (**), bone fr. and tooth fr. (****) with thermoalteration traces, fat-char (*), herbivorous dung (*), carnivorous dung (*), malacological fr. (*), flint fr. (*).	Dark brown (PPL) clays, calcitic crystallitic b-fabric, and undifferentiated b-fabric.	Impregnations of Fe (hydr) oxides (++) and stain in the bones (++), clay coatings (++), calcitic hypo/coatings (++), yellow cryptocrystalline hypocoatings (+), ellipsoidal fecal pellets (+++), granular bioaggregates (+++), calcified filament infillings (++).
H (III-II) S.3, E-5	MU.25 (top S.3). Gravels with silty sands.	Lenticular/platy. 20% porosity.	c/f 50 μm 2/1	Chitonic/monic	Pisolithic-oolitic limestone (****)(SR-SA and tabular) and frost cracks.	Quartz and feldspar (**) (SA) and calcite.	Charcoal fr. (**), bone fr. (**).	Brown (PPL) clays, calcitic crystallitic b-fabric.	Impregnations of Fe (hydr) oxides (+), traces of dissolution and vertical arrangement of limestone (+++), $CaCO_3$-sparitic-coatings in bones (+), fine material coatings (+++).
H (III-II) S.2 and S.1, A-3	MU.26 (S.2 and bottom S.1). Silty sandy gravels with silt capping.	Intergrain microaggregate/granular. 30%–35% porosity.	c/f 50 μm 3/1	Chitonic/concave gefuric	Pisolithic-oolitic limestone (****) (SR, tabular).	Quartz and feldspar (**) (SA) and calcite.	Charcoal fr. (*), bone fr. (**).	Brown (PPL) clays, calcitic crystallitic b-fabric.	Silt cappings (++++), clayey silt infillings (++) clay coatings (+++), traces of dissolution and vertical arrangement of limestone (+), impregnations of Fe (hydr)oxides (+), micritic $CaCO_3$ coatings appear in the porosity of spongeous bones(++).

Abbreviations: AL, archaeological level; AOM, amorphous organic matter; Fr, fragments; MU, microunit; S, sample; Shape: A, angular; R, rounded; SA, subangular; SR, subrounded.

Class frequencies (after Bullock et al., 1985): *Very few (<5%); **Few (5%–15%); ***Frequent (15%–30%); ****Common (30%–50%); *****Dominant (50%–70%); ******Very dominant (>70%).

Class abundance of pedofeatures after (Bullock et al., 1985): +Rare (<2%); ++Occasional (2%–5%); +++Many (5%–10%); ++++Abundant (10%–20%); +++++Very abundant (>20%).

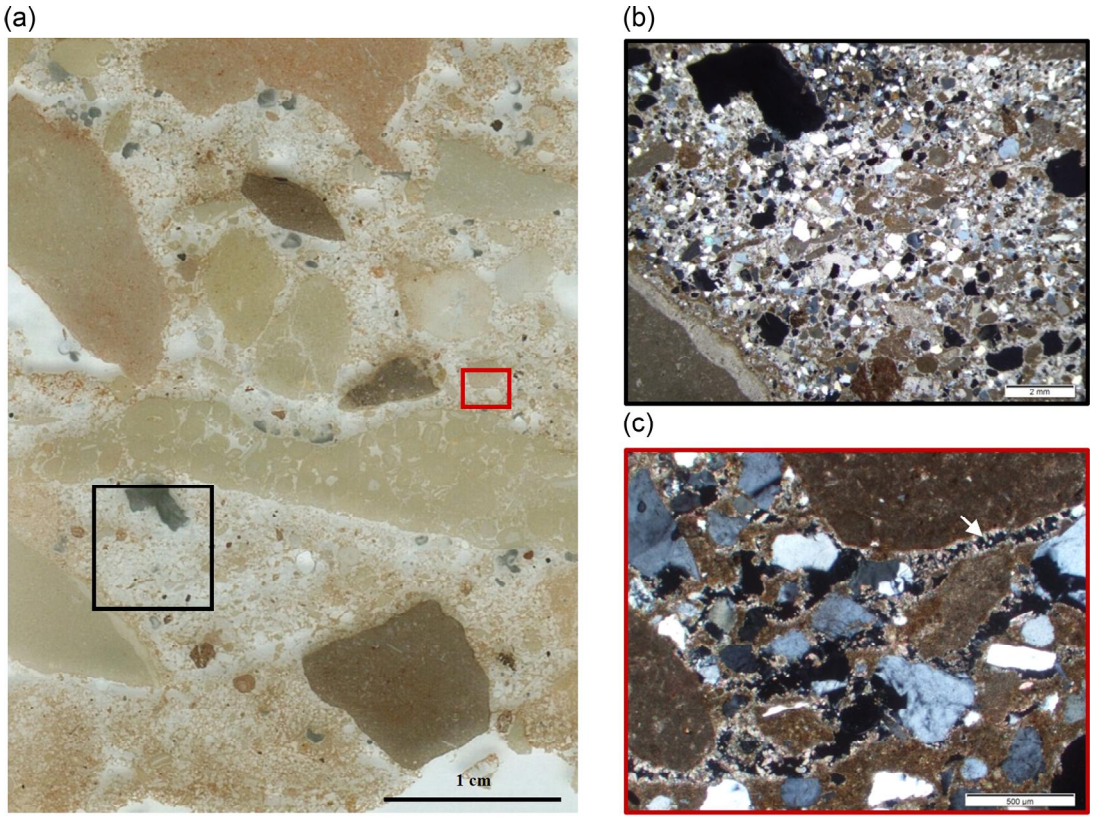

FIGURE 7 Unit A (AL IX) MU.1/Sample 18. (a) Transmitted light scan of part of the thin section with subrounded cobbles and pebbles in sands. (b) Cemented coarse and medium sands XPL in the black box in (a). (c) Calcitic depletion zones and calcitic coatings (white arrow) mainly in sands XPL in the red box in (a). MU, microunit; XPL, crossed-polarized light.

personal communication, 12th June, 2021, Institut d'Arqueologia [IAUB]). The fine fraction is composed of mainly sandy silty clays with a channel/granular microstructure and the presence of vesicular voids and a matrix-supported fabric. Discrete laminations of fine material appear among the groundmass (Figure 10d). There is an increase in almost whole gastropod remains (Figure 11a) and a considerable decrease in charcoal and bones compared to the previous unit, although there is some fat-derived char (Figure 11b), a residue produced from the burning of meat, bone, and/or animal fat and characterized by numerous vesicles with small fissures or cracks radiating from the walls (Mallol et al., 2017; Villagran et al., 2017). Silica phytoliths and some spores (Figure 11c) are found scattered throughout the groundmass. The pedofeatures from biological soil activity include calcitic hypocoatings and dense incomplete phytomorphic calcite infillings (queras) (Figure 11d). There is also high lumbricid activity manifested by chamber formation and biogenic calcite granules.

In Unit E (AL VI), several MU are found in three groups:

1. *Sands, unsorted*: This includes MU.5 and MU.6. Dominance of fine to medium sands consisting mainly of quartz and subangular gravels of pisolithic and oolitic limestone (Figure 12a). Some micritic hypocoatings appear on the gravels. Toward the top, MU.6, there is a decrease in cobbles and dominance of subrounded fine sands with clayey silts giving rise to some laminations <1.5 mm thick. Concentric orthic nodules of iron oxides and hydroxides appear.
2. *Sands with a tendency to be well sorted*: This includes MU.7 to MU.14. In general, fine to medium sands (Figure 12b)—MU.7, 9, 10, 11, 12, and 14—mainly composed of subangular to subrounded quartz and, to a lesser extent, micritic limestone, some clay aggregates, especially in MU.14, and some chert. They can appear, as in MU.10 and MU.12, with laminations of very fine sands (Figure 12c). Coarse to very coarse sands are also found in MU.8 and MU.13 (Figure 12d), composed of subrounded to rounded micritic limestone, quartz, muscovite, and aggregates of red clays.

Despite the particle size of the different MU, it is worth highlighting their composition, in which, apart from quartz and mica and in some cases chert, micritic limestones also appear repeatedly in the current bed of the ephemeral stream (rambla), as well as in the alluvial profiles. The subrounded aggregates of silty clays (*terra rossa*) from the limestone formations that can currently be seen in the bed of the rambla are also noteworthy.

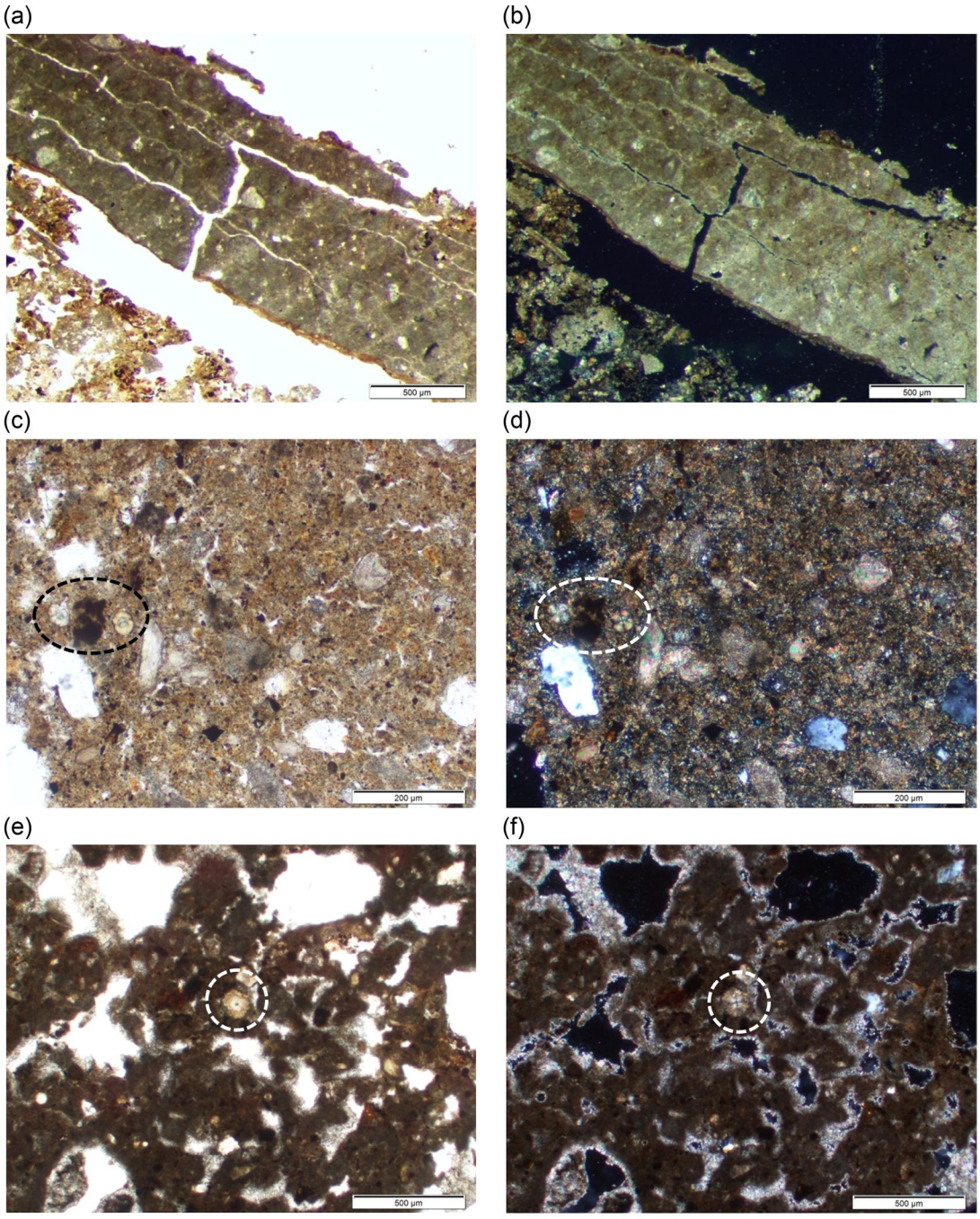

FIGURE 8 Unit C (AL VIIIa). (a) MU.3/Sample 12a. Cracked in situ platy clasts of limestone in PPL. (b) Same as (a), in XPL. (c) MU.3/Sample 16. Phosphatized clayey and silty fine material with spherulites in the dashed circle on either side of charcoal residues, in PPL. (d) Same as (c), in XPL. (e) MU.3/Sample 16 Calcite-rich groundmass with spherulite in the dashed circle, in PPL. (f) Same as (e), calcitic crystallitic b-fabric, in XPL. MU, microunit; PPL, plane-polarized light; XPL, crossed-polarized light.

3. *Clayey silts with fine sands*: They are located at the top of the sequence and are represented from MU.15 to MU.18. They are characterized by a greater contribution of clayey silts, which gradually increase toward the top of the sequence. Moreover, they have a greater sedimentary thickness, especially MU.17 (Figures 12e) and 18. Sandy silt laminations appear in the latter. The lithological and mineralogical composition does not differ from the two previous groups described, but some plant residues are found and it is especially distinguished from the others by a series of features such as calcitic hypocoatings in voids, faunal passages, fecal pellets, clay coatings in voids, and in the detrital material.

Unit F (AL V) is formed by subrounded to subangular cobbles and gravels of pisolithic-oolitic limestone in a matrix of silty clays and a matrix-supported fabric. The gravels show traces of dissolution.

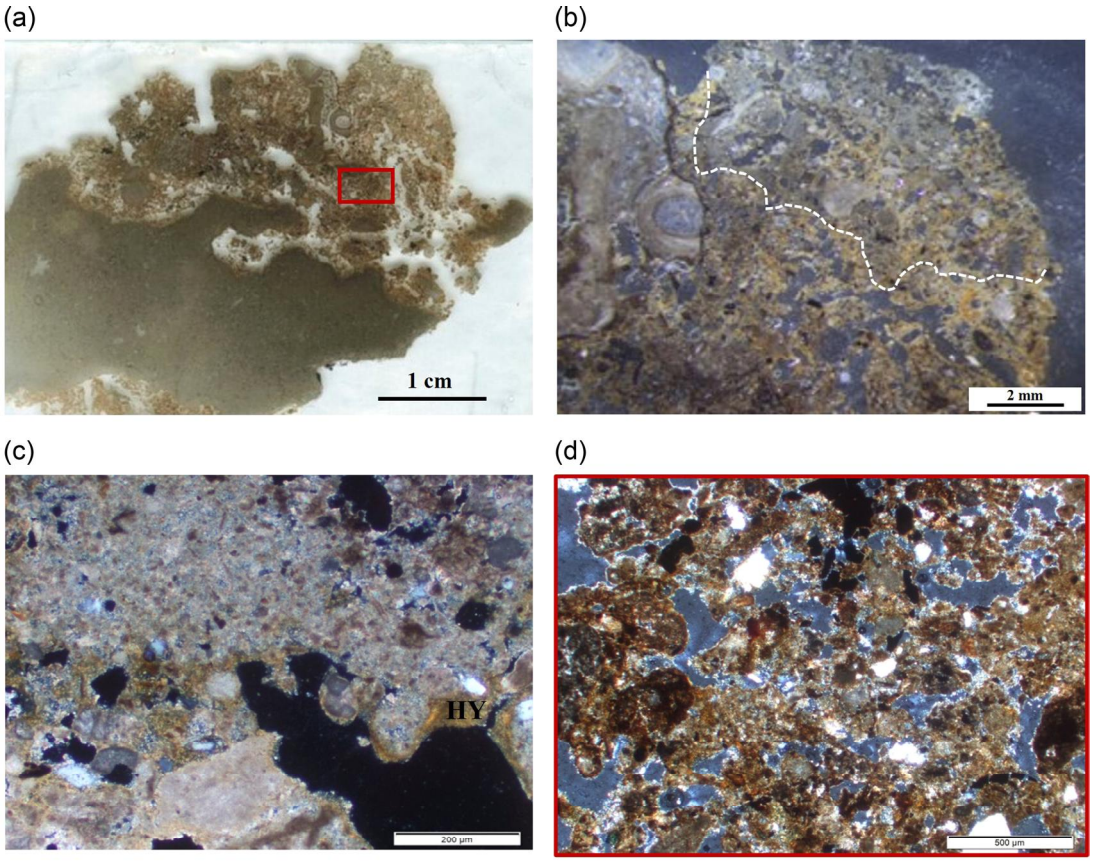

FIGURE 9 Unit C (AL VIIIa), Sample 12b, Hearth. (a) Overview transmitted light scan. (b) At the top, calcitic ashes in OIL are shown. (c) Detail of (b) with some calcium carbonate pseudomorphs of prismatic forms and hypocoatings (HY) of fine material, in XPL. (d) Slight traces of thermoalteration in the groundmass with some charcoals in the red box in (a), in XPL. OIL, oblique incident light. XPL, crossed-polarized light.

There is an increase in fragmentary charcoal, bone, and flint in relation to the previous units.

Two MU have been distinguished: MU.19 has a vughy, vesicular microstructure with traces of calcitic depletion in the groundmass, some calcitic coatings in gravels, and dense or loose microsparitic infillings. MU.20 is characterized by a granular, crumbly microstructure in some areas and by silty–clay coatings around the gravels. Amorphous residues of organic matter and silica phytoliths are more abundant in MU.20. There are also dense incomplete infillings of phytomorphic calcite (queras), channels, calcitic hypocoatings, and aggregates and voids typical of soil faunal activity.

Unit G (AL IV) is generally characterized by a vughy and channel microstructure with a matrix-supported fabric of silty clays with fine sands. There are some subrounded gravels with traces of dissolution. Laminations of very fine material are found (Figure 13a), sometimes consisting of charcoal and/or organic residues (Figure 13b). There is a considerable increase in archaeological remains in the groundmass. Particularly noteworthy are the remains of bones and teeth with various traces of combustion, yellow to orange-reddish in PPL, and with some fissures, as well as brownish-black partially carbonized organic matter residues in PPL and black woody fragmenting charcoal with the presence of calcium oxalates (Figure 13c,d). The biological activity of the soil fauna is highlighted by the presence of ellipsoidal mite droppings in channels (Figure 13e), calcitic hypocoatings, and dense incomplete infillings of phytomorphic calcite (queras) in the voids of the groundmass (Figure 13f).

Several MU can be distinguished, which can be grouped into two according to their pedosedimentary features:

1. Silty clays with $CaCO_3$. This would include MU.21 and MU.23 (Figure 14a,b). They are especially distinguished by their partially cemented micritic groundmass. In MU.23, there are some fragments of ash and charred remains that are in an advanced state of disintegration.

   The bones, mainly those of a spongy structure, appear with $CaCO_3$ infillings and hypocoatings in the pores (Figure 14c) and on their edges. There are some yellow cryptocrystalline hypocoatings in PPL in the detrital material.

   In MU.23, a combustion area in grid square G-3 (Figure 14d) was located in the thin section (Sample 19), in which it was distinguished from top to bottom (Figure 14e): 3.5-mm-thick calcitic ashes, which are slightly phosphatized, making it practically isotropic in some zones. Some brown to brownish gray bone fragments appear (Figure 14f) with bubble-shaped pores. The microstructure is massive/vughy with an open porphyric-related distribution. There are some predominantly fine sand and quartz

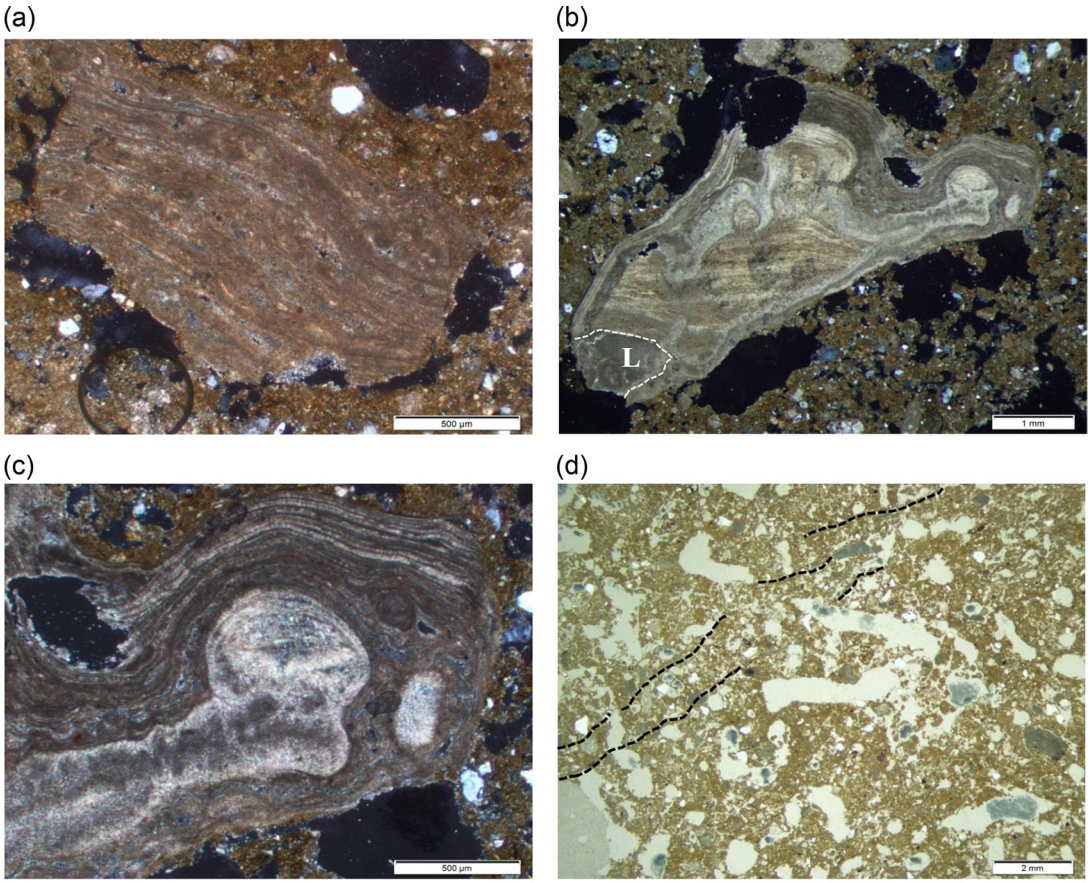

FIGURE 10 Unit D (AL VII) MU.4/Sample 13. (a) Fragment of concretion in the groundmass with banded laminations, some lighter-colored micritic and some darker, more detrital, in XPL. (b) General view of a concreted limestone fragment, L, in XPL. (c) Same as (b) in detail. Microcrystalline fabric, laminated and with a palisade or columnar habit in which the growth tips of the crystals are visible, in XPL. (d) General view of laminations, marked with dashed lines, in a bioturbated groundmass, in PPL. MU, microunit; PPL, plane-polarized light; XPL, crossed-polarized light.

particles. At the bottom, partially cemented silty clays appear. It is distinguished by the occurrence of orthic nodules and impregnations in the groundmass of Fe oxides and hydroxides (see Figure 14e).

2. Silty clays with organic and charcoal residues (Figure 15a) comprise MU.22 and MU.24. Amorphous organic residues dominate together with remains of woody charcoal in the process of disintegration, some of them partially charred (Figure 15b); some appear with a filiform morphology. Silica phytoliths (Figure 15c) and ashy aggregates are scattered in the groundmass (Figure 15d), especially in MU.24.

In the bone remains that are abundant in these MU, some are found with in situ fissures that give rise to articulated and slightly displaced fragments (Figure 16a). Some bone remains appear with traces of combustion, mostly reddish-brown with black contours in PPL (Figure 16b) and fissures; others appear with staining showing a reddish hue in PPL (Figure 16c) and with traces of dissolution (Figure 16d), leading eventually to their fragmentation; and finally, others appear with calcified filament infillings (Figure 16e,f). Some fat-derived char also present.

In MU.22, there are fragments of coprolites distinguished by their tabular morphology, 2–3 mm, formed by an optically isotropic yellow phosphate cryptocrystalline accumulation with an undifferentiated groundmass (Figure 17a–c). They contain some silica phytoliths, as well as some bone fragments with some mineral particles. They show stains and pigmentations of Fe oxides and hydroxides from 25 to 40 µm. All these features correspond to animals with a carnivorous diet (Brönnimann, Pümpin, et al., 2017), some of which show vertical fissuring.

In MU.24, there are some <1 mm fragments of coprolite with incipient fragmentation (Figure 17d). Inside, there are fecal spherulites and disarticulated silica phytoliths (Figure 17e,f), suggesting that they belong to an animal with a herbivorous diet (Brönnimann, Ismail-Meyer, et al., 2017). There are also several flint fragments. Among the pedofeatures of these MU, we highlight Fe oxide and hydroxide impregnations in the groundmass as a result of thermoalteration, especially in MU.24.

Unit H (AL III and II) is mainly composed of gravels of tabular morphology with a subangular and subrounded tendency of the clast-supported type. Two MU have been distinguished—MU.25 and

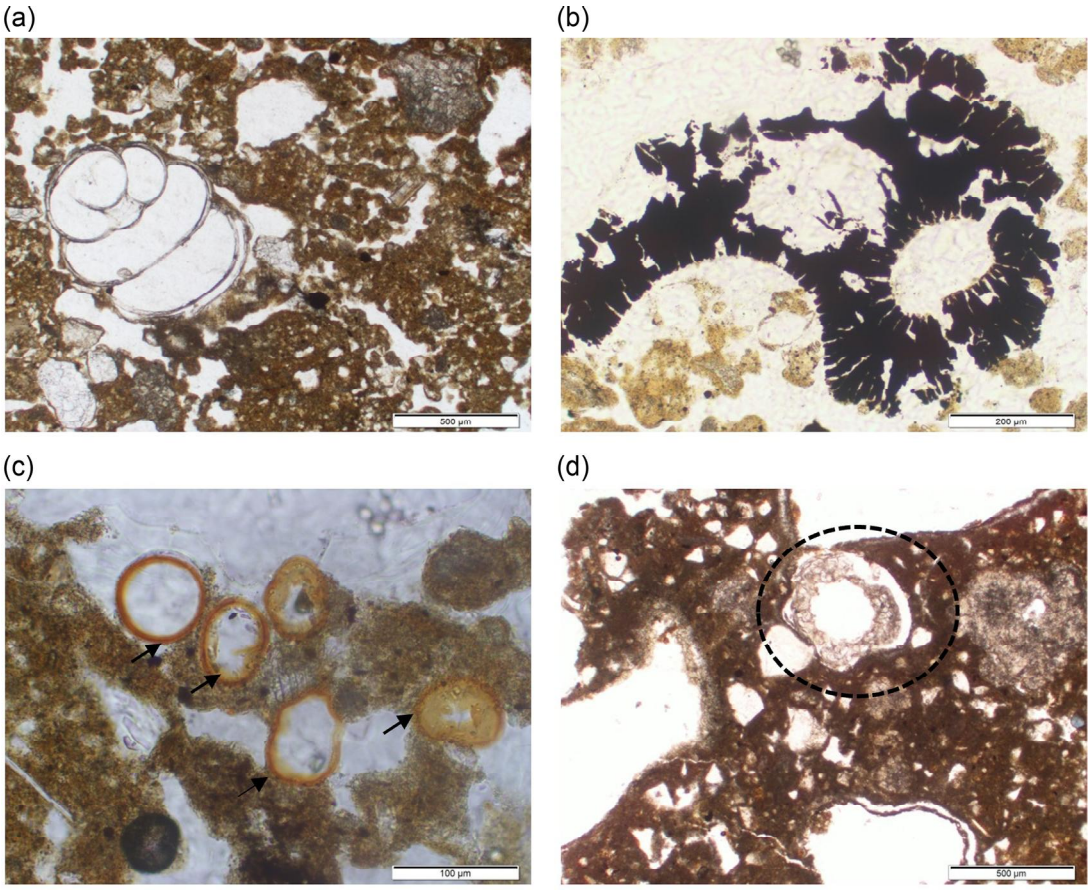

FIGURE 11 Unit D (AL VII). (a) MU.4/Sample 14, practically whole gastropod, in PPL. (b) MU.4/Sample 13, fat-derived char, in PPL. (c) MU.4/Sample 13, arrow-marked spores scattered in the groundmass, in PPL. (d) MU.4/Sample 14, dense incomplete phytomorphic calcite infilling (quera) in a dashed circle, in PPL. MU, microunit; PPL, plane-polarized light.

MU.26—in which differences exist in the microstructure and pedofeatures. It should also be noted that both MU show a decrease in anthropogenic components with respect to Unit G, although in MU.25, they are more abundant. There are well-preserved woody fragments, some of which show ring-porous and tracheid structures (Figure 18a). The latter is typical of coniferous species. Bone fragments and flint elements are also found.

MU.25 is characterized by a microstructure with a lenticular–platy tendency (Figure 18b) and by a fissure in the detrital material, and sometimes, traces of dissolution with a slightly vertical orientation (Figure 18c). In contrast, MU.26 is distinguished by an intergrain microaggregate and granular microstructure (Figure 18d) and pedofeatures that include fine material coatings on top of or around the detrital material in the form of silt capping (Figure 18e), some coatings and infillings of fine material in voids, and detrital material (Figure 18f).

In the located combustion area within Unit H (AL III), the following features have been distinguished (Figure 19a): a layer formed by calcitic ashes, with a platy and lenticular microstructure showing "banded fabrics" (Figure 19c), and the presence of mainly fine quartz sands and some gravels of micritic and oolitic limestone. There are abundant, grayish-colored bones in PPL, some of them vertical with fissures. Articulated silica phytoliths are also present (Figure 19d). Pedofeatures include some silt cappings among the aggregates and among the bone fragments, and localized sparitic calcitic infillings causing fragmentation of the bone remains. The lower part is composed of silty clays with orthic nodules of iron oxides and hydroxides, and reddish-brown plant residues are also observed in PPL in a partially carbonized horizontal arrangement (Figure 19a,b), most likely bark (Ismail-Meyer, 2017). Some elongated silica phytoliths are present.

5 | DISCUSSION

5.1 | Geogenic record: Depositional and postdepositional processes

The sedimentary dynamics of the site begins with Unit A (AL IX), with coarse and medium sands with subrounded cobbles, the infilling of the bar or the channel of the Rambla de Ahíllas. It is an episode of alluvium with local cobbles as a product of bed scouring, with moderate to high hydraulic energy, typical of flash flood with a nonuniform regime. This unit indicates a phase of alluvial activity with

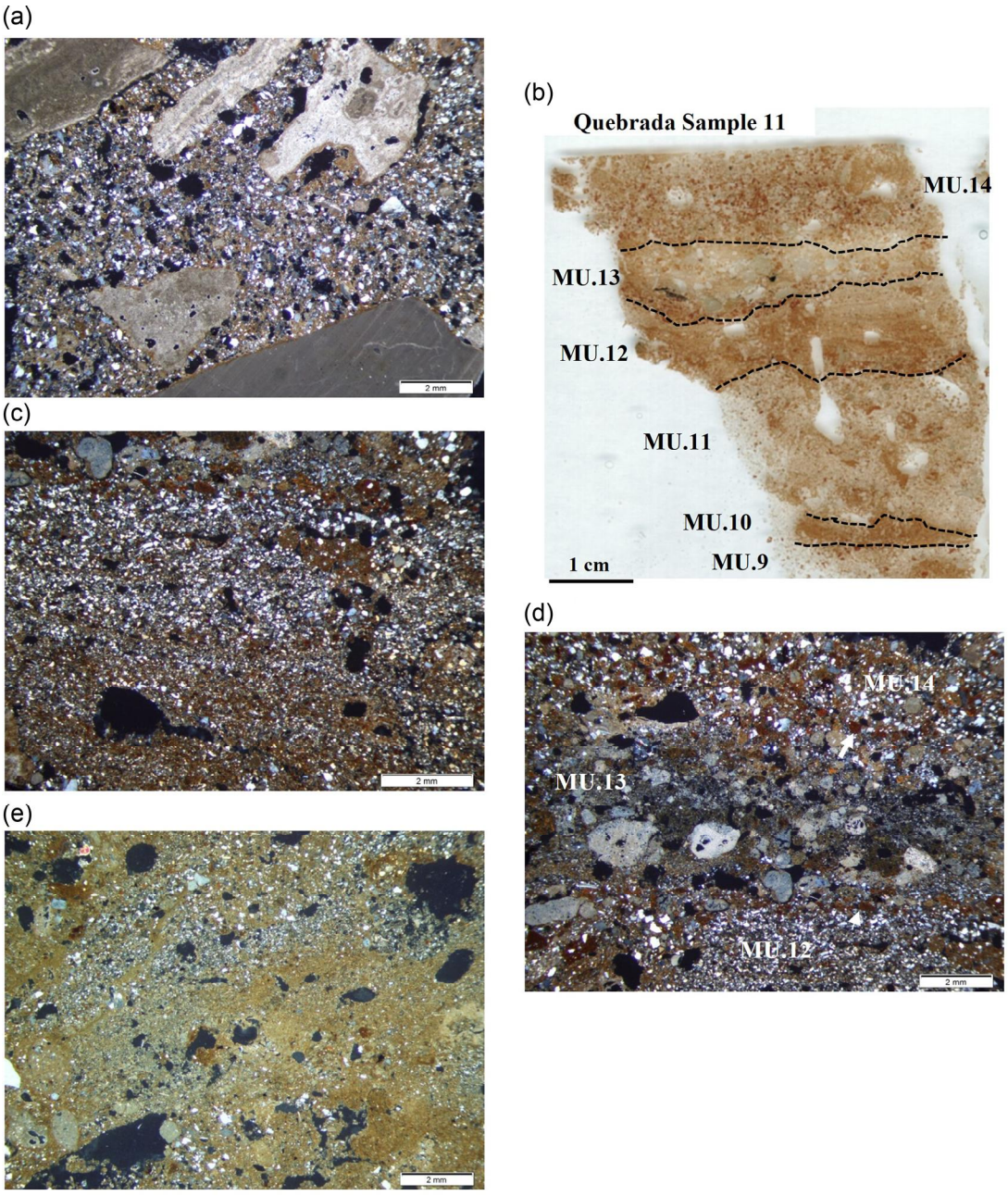

FIGURE 12 Unit E (AL VI). (a) MU.5/Sample 15, fine to medium sands with subangular limestone gravels, in XPL. (b) Sample 11, overview of granoclassified sands—MU.10, 11, 12, 13, and 14—transmitted light scan. (c) MU.12/Sample 11, lamination of very fine, well-sorted sands, in XPL. (d) MU.14–MU.13–MU.12/Sample 11, general view of red clay aggregates (arrow) and micritic limestone sands in MU.13, in XPL. (e) MU. 17/Sample 9, clayey silt with some voids likely due to biological activity, in XPL. MU, microunit; XPL, crossed-polarized light.

high sediment loads suggestive of a possible decrease in vegetation cover and an increase in erosion and consequent sediment production. The bed of the ephemeral stream penetrated the rockshelter itself. Some reworked archaeological remains can be found.

Subsequently, microsparitic-type calcium carbonate crusting occurred. Some traces of dissolution and recrystallization are observed, a feature that may occur from the parent material itself due to the translocation of bicarbonates in the water circulating through the system (Boixadera & Poch, 2008). Hardening and cementation of the horizon would have occurred as a result of successive dissolution/reprecipitation processes and also because it is in contact with the limestone substrate of the rockshelter, which does not facilitate drainage.

After a sedimentary interruption, Unit B (AL VIIIb and VIIIc) is represented by a thin intercalation of angular gravels and cobbles, with laminations of fine to medium sands. This corresponds to an episode formed by local debris and alluvial contributions from the rambla that reactivates the transport of course sediments, but not with as much energy as in the previous unit. These dynamics were intermittent, as suggested by features such as $CaCO_3$

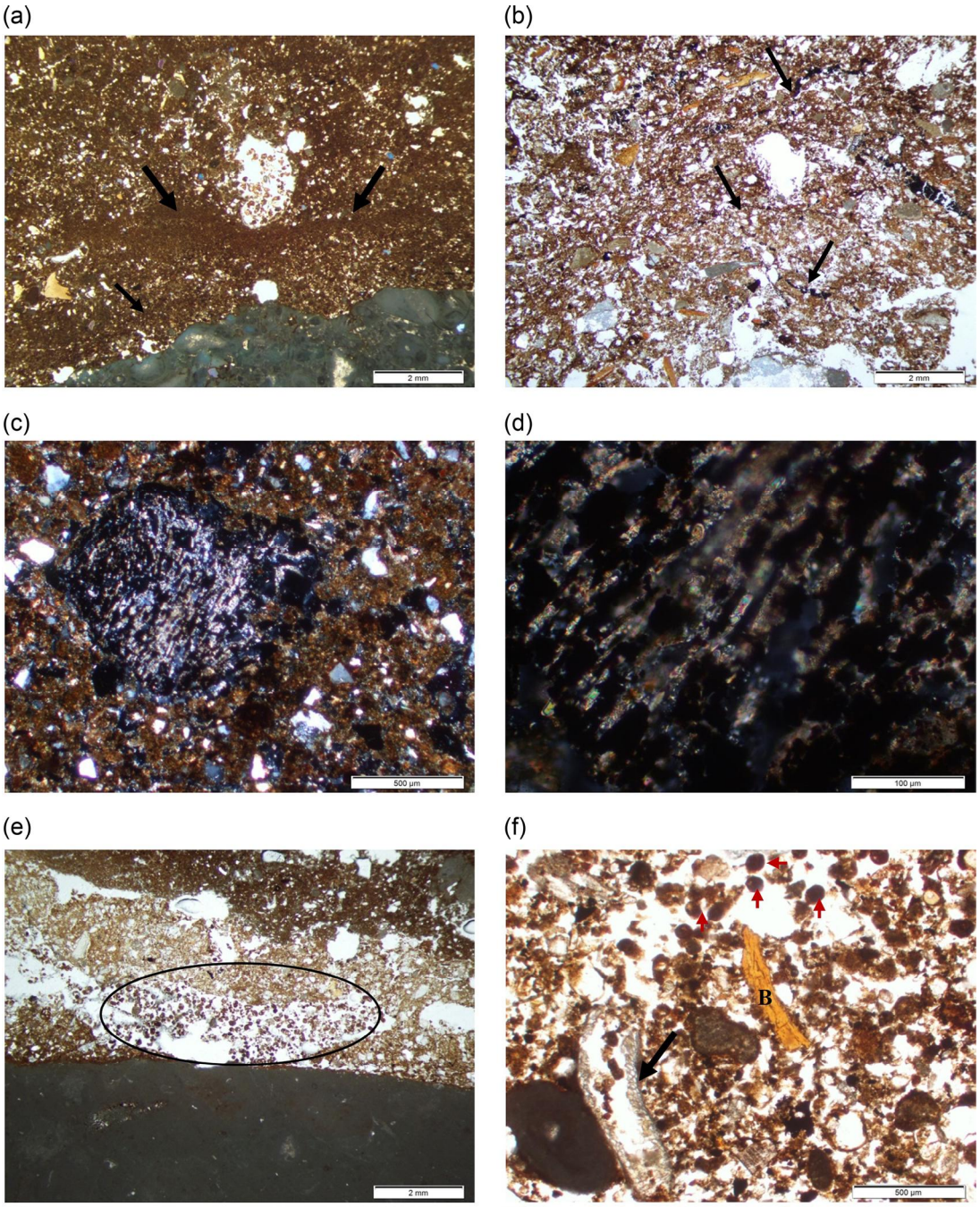

FIGURE 13 Unit G (AL IV). (a) MU.23/Sample 20, clayey silt laminations between the groundmass marked with arrows, in PPL. (b) MU.22/Sample 6, organic/charcoal residues laminations marked with arrows, in PPL. (c) MU.22/Sample 4, wood charcoal and associated calcium oxalate crystals, in XPL. (d) MU.22/Sample 4, detail of calcium oxalate crystals, in XPL. (e) MU.23/Sample 20, loose continuous infilling with mite excrement, ellipse, in PPL. (f) MU.22/Sample 6, dense incomplete infilling of phytomorphic calcite (quera) with a black arrow, B (bone) and mite excrement, with red arrows, in PPL. MU, microunit; PPL, plane-polarized light; XPL, crossed-polarized light.

hypocoatings that appear in the voids as a result of calcium carbonate precipitation due to root metabolism (Durand et al., 2010), thus corroborating episodes of ephemeral stream inactivity. As in the previous episode, there is some crusting and recrystallization, but not as pronounced. There is a slight increase in archaeological remains, most likely due to more favorable living conditions at the site.

Unit C (AL VIIIa) corresponds to an episode with different processes in its formation. First, frost action resulted in fragmentation of the limestone material of the rockshelter walls and roof into coarse clasts. Some of the large clasts have an angular and platy morphology. There are also boulders from the rockshelter roof that induced a change in the morphology of the settlement, followed by a solifluidal displacement of the materials, inducing lobes with

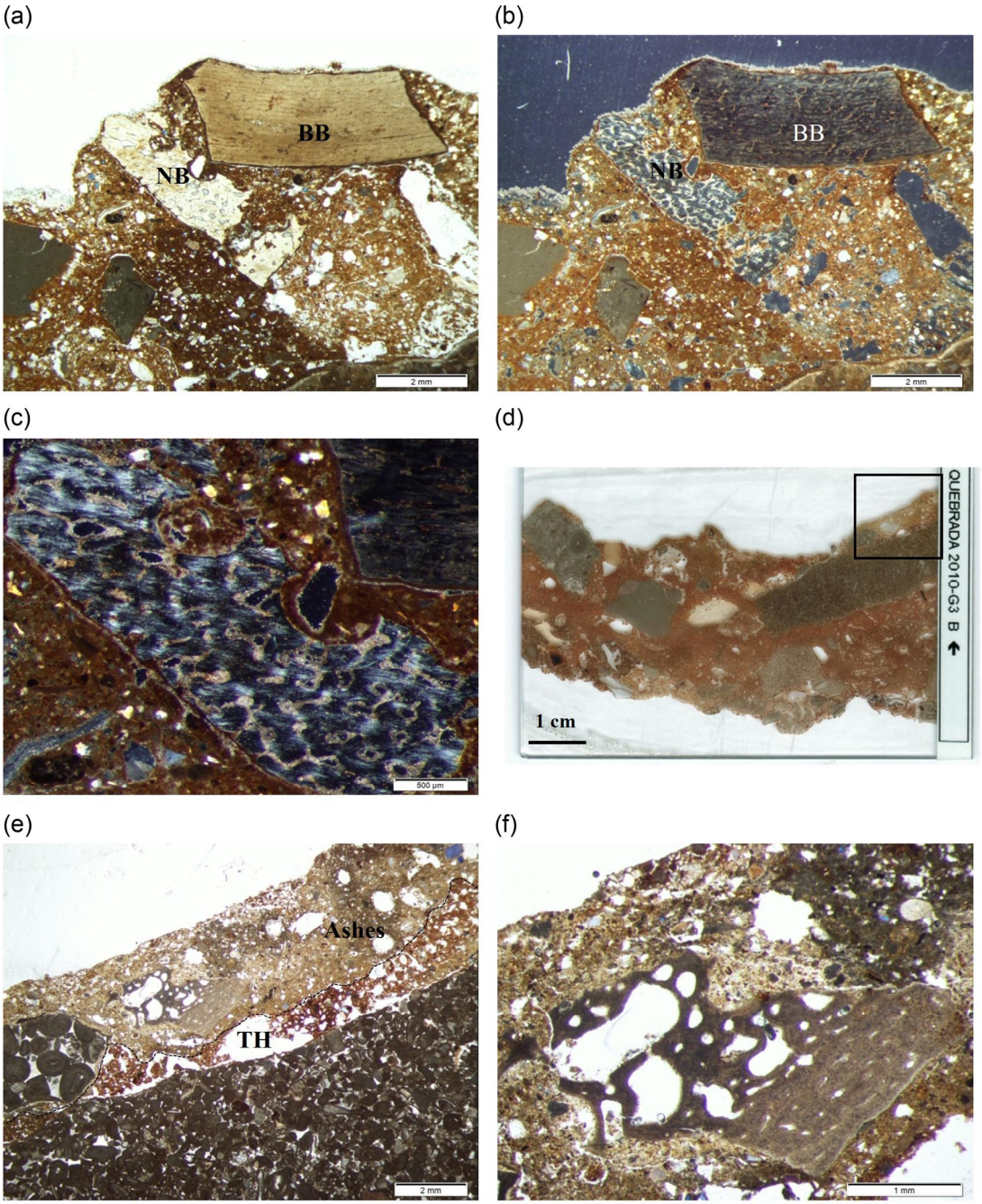

FIGURE 14 Unit G (AL IV). (a) MU.23/Sample 20, overview of the $CaCO_3$-bearing silty clay-type microunits in which bones, burnt (BB) and unburnt (NB), are observed, in PPL. (b) Same as (a), in XPL. (c) Detail of the previous bone, in which $CaCO_3$ infillings and hypocoatings are observed in the pores, in XPL. (d) MU.23/Sample 19, general view of the thin section from the black box part of the hearth. Transmitted light scan. (e) Detail of (d), view of the hearth: upper, calcitic ashes, slightly phosphatized, and lower, thermoaltered silty clays (TH), in PPL. (f) Detail of (e), brown to brownish gray bone (calcined) and bubble-shaped pores due to high combustion, in PPL. MU, microunit; PPL, plane-polarized light; XPL, crossed-polarized light.

well-developed preferential orientation of clasts, some of which show vertical or inclined changes in orientation because of repeated movements and variations due to freeze–thaw processes. Occasionally, some are fissured in situ, all indicating a cooling climatic episode.

In the E-G-I/3-6 sector of the rockshelter, where the clast fraction is more abundant, there is the formation of laminar calcrete crusts consisting of a dark-colored micritic band with calcite spherulites. Its genesis has been suggested to be due to the biogenic activity, most likely of cyanobacteria and bacterial mats that developed as thin films in wet environments and subsequently dried out, meaning that they must form at the sediment/atmosphere interface (Alonso-Zarza & Wright, 2010; Durand et al., 2010;

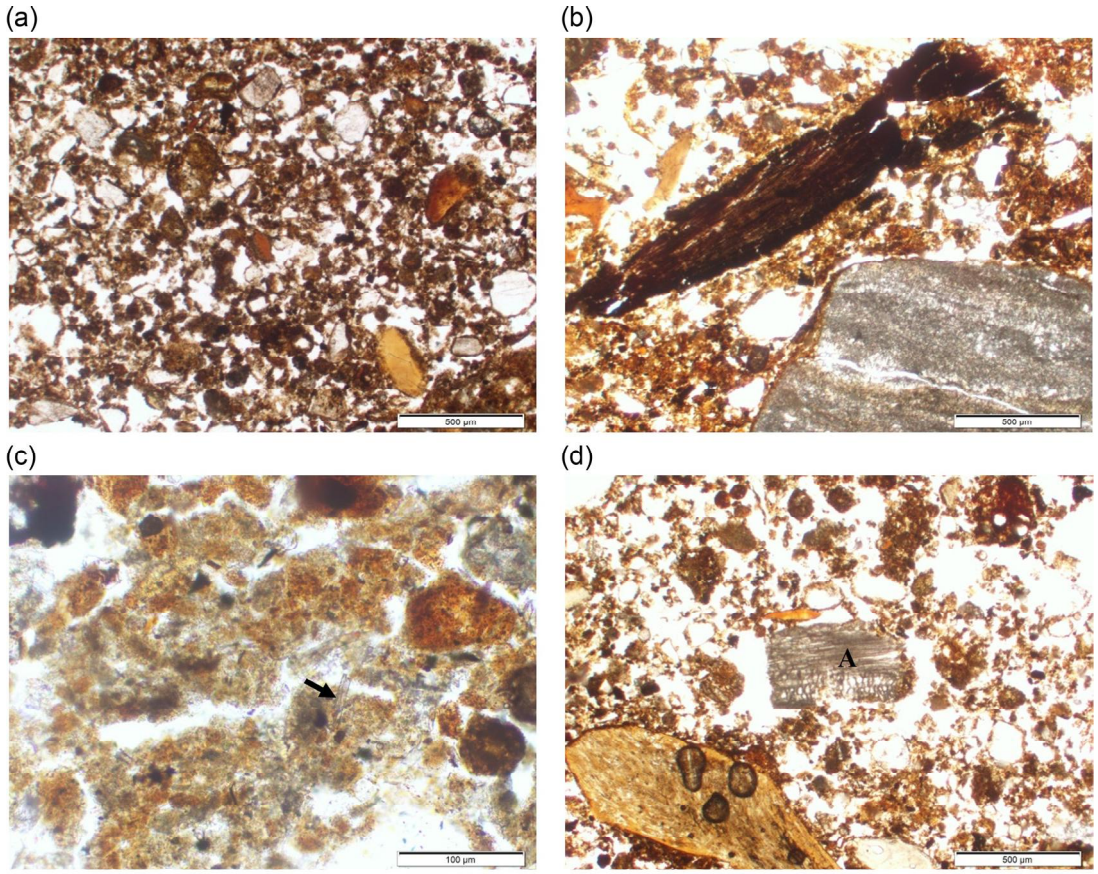

FIGURE 15 Unit G (AL IV). (a) MU.22/Sample 4, silty clays with fine organic material, in PPL. (b) MU.24/Sample 5, partially charred woody fragment, in PPL. (c) MU.24/Sample 5, silica phytoliths distributed in the groundmass with an arrow, in PPL. (d) MU.24/Sample 5, ash fragment (A) distributed among the groundmass, in PPL. MU, microunit; PPL, plane-polarized light.

Verrecchia et al., 1995). We propose that its origin in Abrigo de la Quebrada in some sectors was favored by the presence of boulders in sectors E-G-I/7-10 that did not facilitate drainage of thaw water and so this bacterial activity developed. This also reveals that Unit C was exposed to the atmosphere for a certain period of time.

Another interesting feature in the same sector is the formation of pendants on the clasts. Their genesis is related to processes of dissolution and precipitation of carbonates, which is accentuated in the lower part of the detrital material as more humidity has been retained (Dorronsoro et al., 2020; Ducloux & Laouina, 1989; Durand et al., 2010). These accumulations appear in the form of layers; the ones closest to the clasts are older and are formed of micritic calcium carbonate and the most recent ones are formed by an increase in detrital material and appear darker. According to Durand et al. (2010), the carbonate-rich laminations form in more arid phases with less biological activity, the latter more typical of a more humid environment; therefore, it also demonstrates certain environmental changes in the same unit that would correlate with the above processes. Finally, we identified illuviation of fine material in voids and gravels that is likely due to liquefaction processes on the surface and/or rapid percolation of surface runoff after thawing (Van Vliet-Lanoë, 2010).

The paleoenvironmental conditions of this Unit C were initially cold and arid, but gradually became wetter as conditions moved toward a less harsh environment.

Unit D (AL VII) is caused by several processes: (a) an episode of rockshelter roof collapse that is particularly reflected in grid squares E/4-5, not as important as in the previous episode, although in E-3, there are still gravels and cobbles from the rockshelter wall, but not as abundant as in the previous episode, and (b) a mass displacement as the coarse material is embedded in a very fine matrix and tends to have an orientation depending on the slope of the deposit (Karkanas & Goldberg, 2019). Some laminations of very fine material are also observed in the matrix as a result of this displacement.

One aspect to consider is that there are carbonate concretions in the cobbles and blocks (see Figure 5a) that did not originate in situ, but are instead from the initial roof or wall of the rockshelter. This feature indicates that between Units C and D, there was a hiatus in which conditions were favorable for the precipitation of carbonates, due to a warm environment and availability of water.

After the formation of Unit D, conditions of stability were established. This is indicated by localized root activity in the form of calcification–decalcification features associated with impregnation of

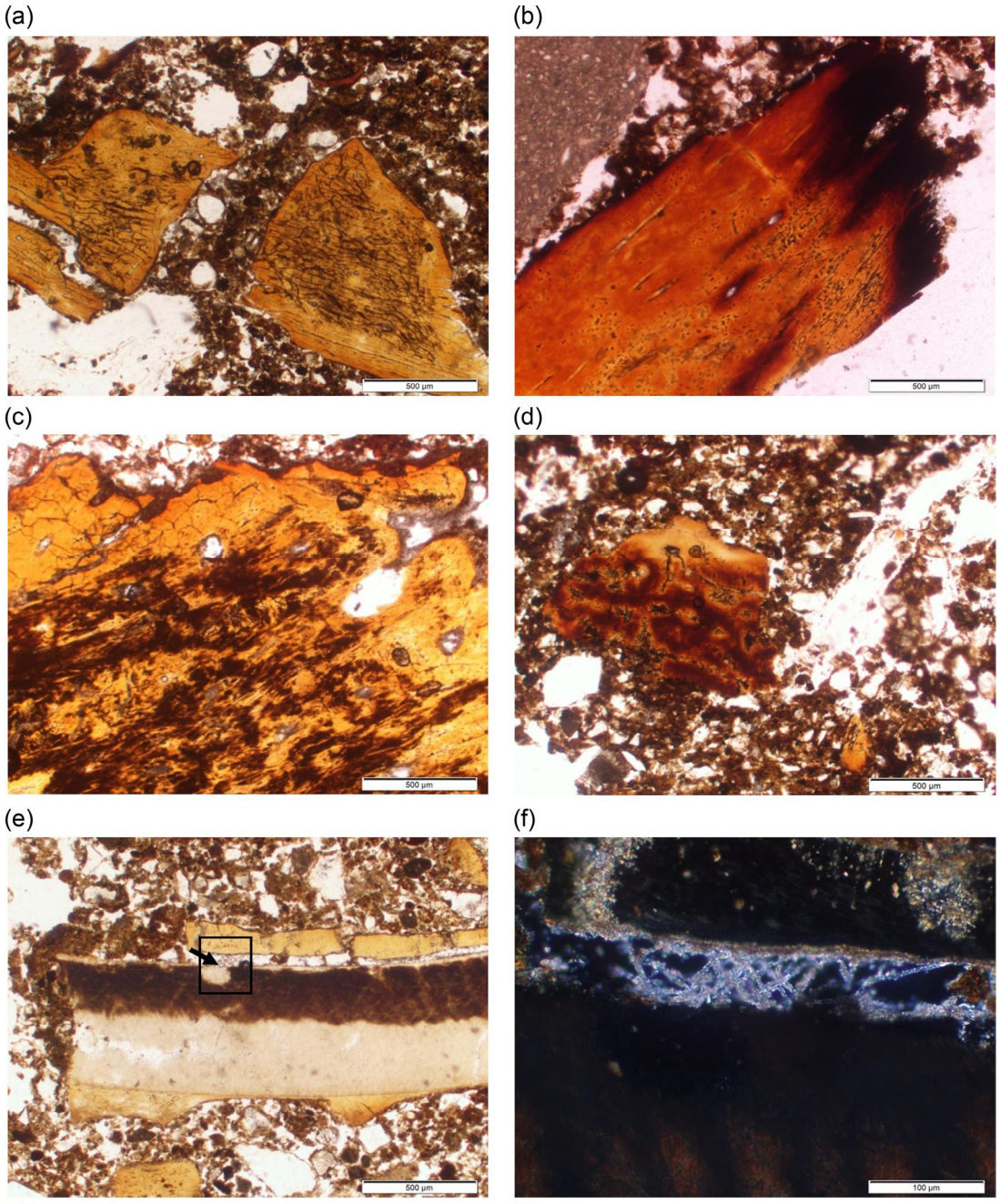

FIGURE 16 Bones in Unit G (AL IV). (a) MU.22/Sample 4, bone fragment probably cracked by trampling; some displacement is observed, in PPL. (b) MU.22/Sample 4, bone with thermoalteration traces with reddish-brown color with black contours, in PPL. (c) MU.24/Sample 5, bone fragment with reddish staining, Fe oxides and hydroxides extending over the surface, in PPL. (d) MU.24/Sample 5, traces of dissolution and fissuring around these reddish impregnations, in PPL. (e) MU.22/Sample 4, fragment of a possible burnt tooth with calcified filament infillings (arrow), in PPL. (f) Detail of calcified filament infilling in the black box in (e), in XPL. MU, microunit; PPL, plane-polarized light; XPL, crossed-polarized light.

root tissues known as queras (Durand et al., 2010), silica phytoliths, and some spores. There is also evidence of biological activity, namely, faunal passages, biogenic calcite granules excreted by earthworms (biospheroids) (Canti, 2017; Durand et al., 2010), and the abundant presence of terrestrial gastropods. All these features suggest that Unit D was subaerially exposed for a period of time and that pedogenesis began.

Unit E (AL VI) is due to the alluvial dynamics of the ephemeral stream, in which different episodes can be distinguished with a sequence generally decreasing in grain size. It can also be seen by the erosive contact in some sectors, as well as by its wavy bedding, which is indicative of this dynamic (see Figure 5b). We located several episodes, among which we distinguish from bottom to top:

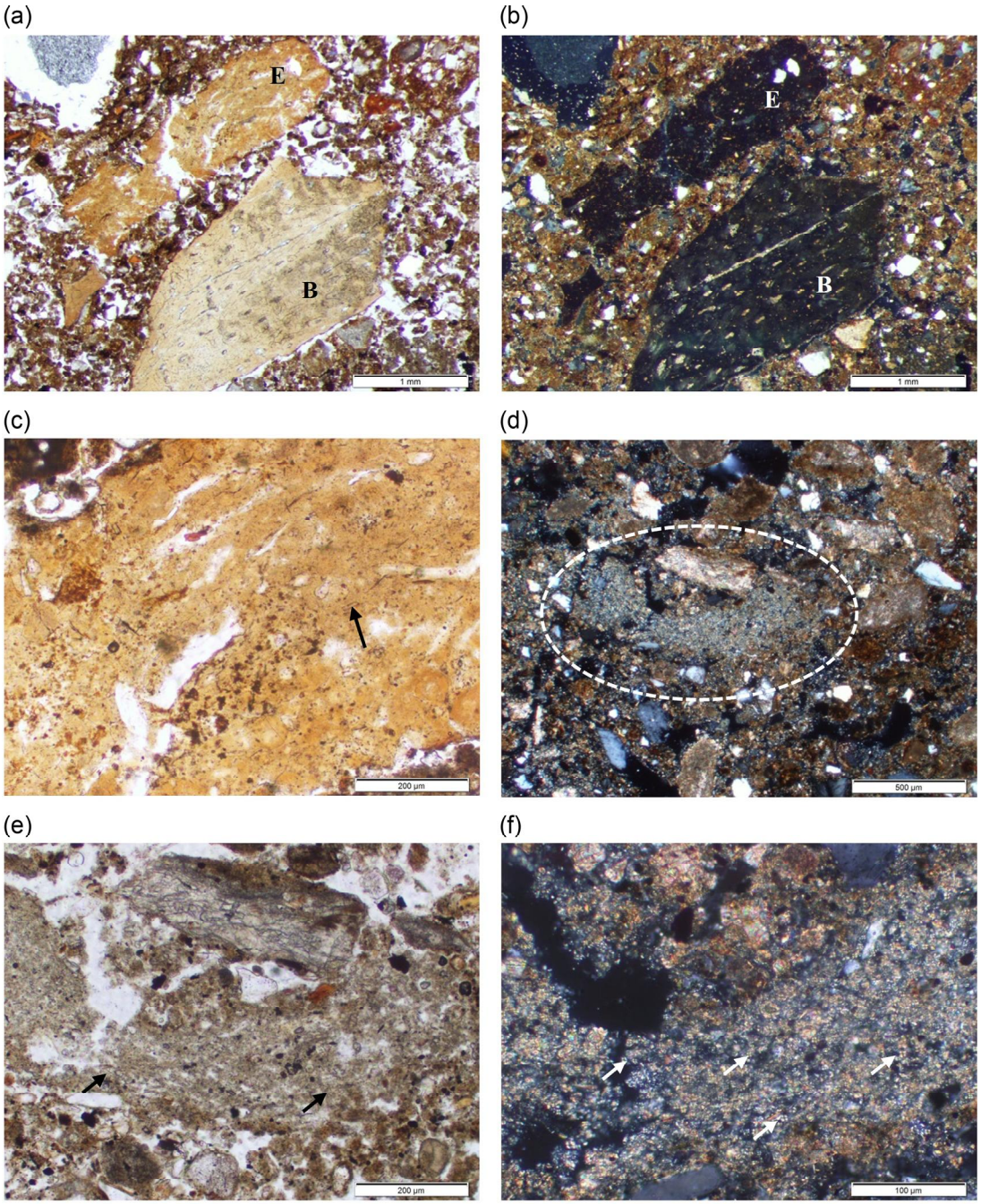

FIGURE 17 Excrements in Unit G (AL IV). (a) MU.22/Sample 4, a bone (B) is distinguished together with an excrement (E) of a suspected carnivorous animal, which is highly phosphatic, slightly fragmented in PPL. (b) Same as (a), but in XPL. Note that the excrement is optically isotropic with undifferentiated b-fabric. (c) Same as (a) in detail. Some silica phytoliths with an arrow, as well as stains of Fe oxides and hydroxides, in PPL. (d) MU.24/Sample 3-bottom-, overview of a fragment of excrement of a suspected herbivorous animal, dashed circle, in XPL. (e) Detail of (d) with some silica phytoliths, arrows, in PPL. (f) Detail of the previous image with numerous fecal spherulites, arrows, in XPL. MU, microunit; PPL, plane-polarized light; XPL, crossed-polarized light.

1. Sands with angular gravels from the dismantling of the previous unit, which could correspond to episodes of higher energy, perhaps of the flash flood type.
2. Well-sorted mainly fine to medium sands denote a low-traction energy environment perhaps in the water recess or could correspond to overflows of suspended load. There are also some episodes of medium to coarse sands without gravel or pebbles, a fact that makes us believe that these correspond to episodes of higher energy.
3. Massive clayey silt corresponding to high-turbidity flood water stagnation with a high concentration of suspended detrital material. This episode is important as it represents an

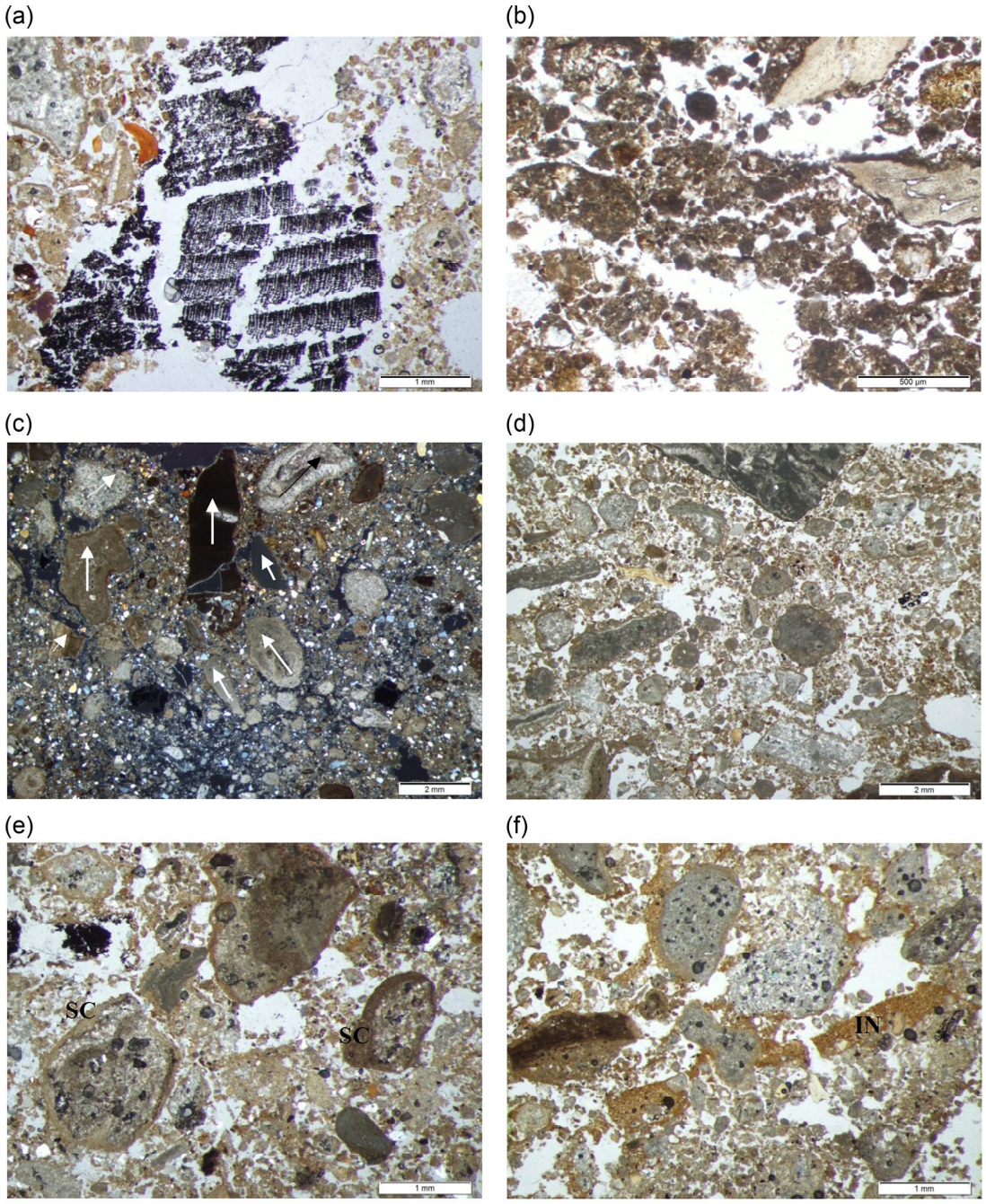

FIGURE 18 Unit H (AL III-II). (a) MU.26/Sample 2, cross-section of conifer wood charcoal in the process of fragmentation. Xylem tissue with vessels (tracheids), in PPL. (b) MU.25/Sample 3—top— microstructure with a lenticular–platy tendency, in PPL. (c) MU.25/Sample 3—top—vertical or inclined orientation of detrital material, marked with arrows, in XPL. (d) MU.26/Sample 2, granular microstructure, in PPL. (e) MU.26/Sample 2, fine material coatings on top of or around the detrital material in the form of silt capping (SC), in PPL. (f) MU.26/Sample 2, clayey silt infillings (IN), in PPL. MU, microunit; PPL, plane-polarized light; XPL, crossed-polarized light.

abandonment of the river bed in the rockshelter at Abrigo de la Quebrada. It shows pedogenesis, since we found biological activity such as roots, soil fauna, and some woody residues, which suggests interruptions in the sedimentary record.

In general, Unit E corresponds to different alluvial episodes with some energy changes, mostly rather low, which may indicate a progressive abandonment of the channel in the deposit. A significant change in sediment supply with less input led to a low erosion rate on the slopes, corresponding to a period under increasing humidity and temperatures with local vegetation coverage. In its final stretch, it functioned as a floodplain. In short, this alluvial dynamic would not be conducive to the occupation of the area of the site.

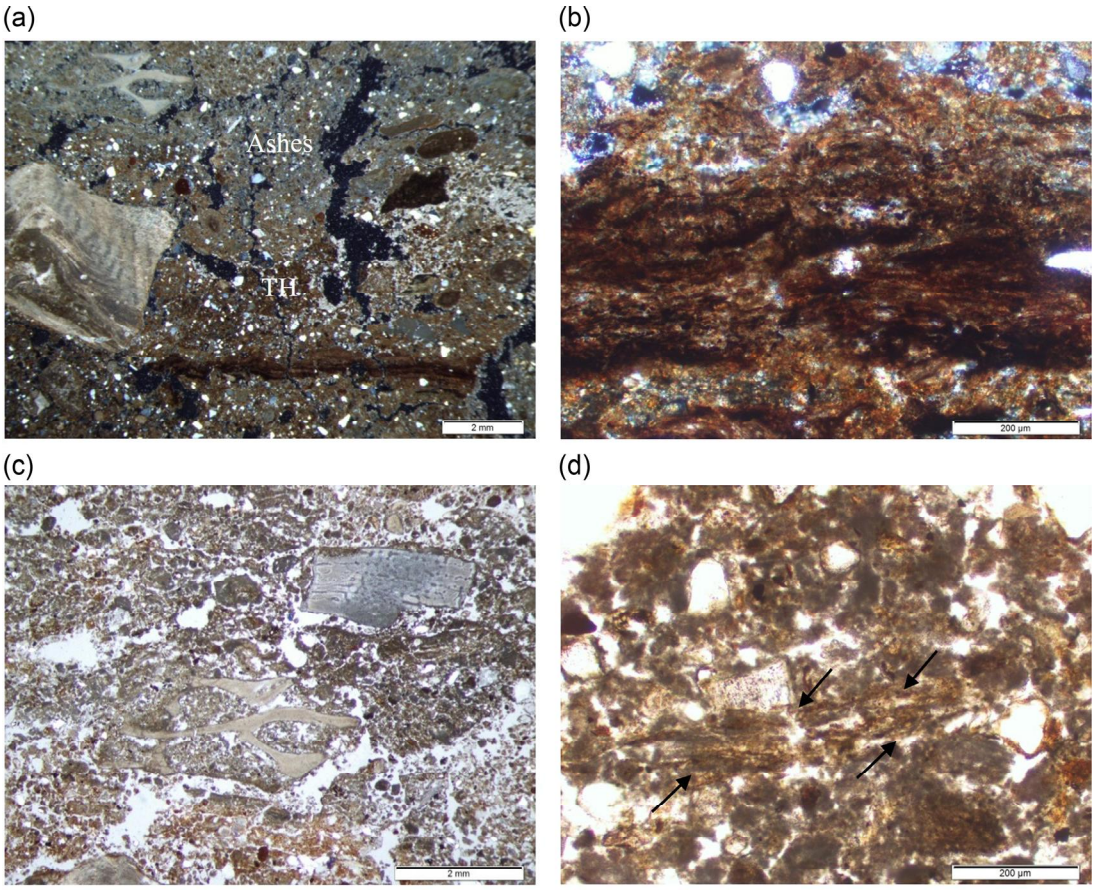

FIGURE 19 Hearth, Unit H (AL III). (a) General view of the hearth, Sample 5: thermoalteration zone (TH), and ashes, in XPL. (b) Detail of the lower part. Horizontal plant residues partially charred, perhaps bark, in XPL. (c) Ash area with banded fabrics with some burnt bone fragments, in PPL. (d) Articulated silica phytoliths, arrows, in PPL. PPL, plane-polarized light; XPL, crossed-polarized light.

From Unit F (AL V) onwards, there are no more accumulations from the Rambla de Ahíllas in the rockshelter. A series of processes were involved in its origin: First, fragmentation of the walls and roof of the rockshelter caused a slope in a northerly direction, especially in the K-3 grid square of the site. Thereafter, some episodes of mass displacement occurred, corroborated by vesicular voids typical of muddy flow liquefaction processes (Bertran & Texier, 1999; Karkanas & Goldberg, 2013). In MU.19, a microsparitic secondary carbonate cementation is observed that may be due to precipitation and evaporation cycles with some traces of dissolution and recrystallization. There is an increase in human activity well recorded in the two MU, although toward the top, MU.20, an episode of stabilization is observed, with an incipient increase in organic matter residues, contrasted also by the important presence of biological activity, including both roots and soil fauna suggestive of pedogenic activity.

Next, Unit G (AL IV) shows a change from the previous units from a sedimentary point of view. This unit is mainly formed by runoff, although some gravels from the fragmentation of the rock still appear in the sectors close to the rockshelter wall.

These diffuse runoff episodes gave rise to laminations that occurred throughout Unit G, even in postoccupation episodes. In this unit, the concentration of organic fine material and plant residues increased compared to the previous unit. These plant residues are burnt and nonburnt and contain silica phytoliths, which, together with the presence of roots (channel microstructure, phytomorphic calcite, and calcitic hypocoating), is indicative of a stabilization episode in the environment. There is also the intercalation of micritic carbonation laminae, especially reflected in MU.21 and MU.23, where carbonate precipitates in the clay micromass fill the spaces between voids. In short, Unit G reflects a phase of low sedimentation that favored strong development of pedogenetic features that appear mixed with human activity.

From this point, there is an abrupt change with respect to the previous Unit, G, characterized by Unit H (AL III and II), which represents the end of the Pleistocene record of the site. This is the result of increased frost-shattered clasts of the walls, and in some sectors, erosive contact at the boundary of Units G and H can be observed. A series of characteristic features of repeated freeze–thaw episodes are found in both the matrix and the coarse fraction. These features include the microstructure with a lenticular tendency, mainly in MU.25, which creates banded fabrics in some zones, frost cracks in the detrital material, and a change in its arrangement to inclined or vertical (Van Vliet-Lanoë, 2010). Accumulations of finer material on

top of the coarse elements—silt cappings—especially in MU.26, would favor their translocation. Another process that is observed is the abundance of illuviated fine material in the form of infillings that can be attributed in this context to liquefaction of the surface during thawing, also located in MU.26 (Van Vliet-Lanoë, 2010).

All these features indicate a major change in the environmental conditions of the rockshelter, which undoubtedly suffered from the frost effects. It is likely that, during drier periods, cryoclastic sedimentation was very active. Later, and even after human occupation, continuous freeze–thaw cycles caused the rotation of aggregates, detrital material, and archaeological material resulting in accumulations typical of gelifluction processes (Van Vliet-Lanoë, 2010). These processes indicate cooling associated with an increase in humidity.

In summary, Unit H (AL III and II) represents a significant shift in environmental conditions in the rockshelter with a marked decrease in ambient temperature.

5.2 | Anthropogenic activity in the sedimentary record

In Abrigo de la Quebrada, Neanderthal activity is evident in practically the entire record from a microstratigraphic point of view, except for Units A (AL IX) and E (AL VI), which have geogenic characteristics not very conducive to the rockshelter's habitability. However, the identification of anthropogenic activity manifests itself mainly in hearths and especially in Unit G (AL IV), where the density of components is considerable.

5.2.1 | Hearths

The hearths analyzed were located in Unit C (AL VIIIa), Unit G, (AL IV), and, finally, Unit H (AL III). They are characterized by their flat or slightly concave morphology, in which it has been possible to identify a single combustion event. The hearths in general consist of rubified sediment overlain by ash and a few associated lithic and bone remains.

In Unit C, a hearth was located in profile E-3, composed of woody tissues and ashes characterized by calcitic accumulation together with some prismatic pseudomorphs of calcium carbonate representative of bark and wood ash (Brochier, 1996). The support shows traces of thermal alteration slightly affected by processes of illuviation of fine material.

In Unit G, a hearth characterized by silty clays with $CaCO_3$ was found in MU.23, specifically in grid square G-3. We can distinguish cemented detrital material with marked traces of thermoalteration. In its upper part, calcitic ashes with calcined bone remains are evidence of a high-intensity fire (Mentzer, 2014).

In Unit H, profile I-5, there is also a hearth in which the fire is established on a detrital layer with moderate thermal transformations together with partially carbonized plant remains and phytoliths that seem to correspond to a previous anthropic activity in Unit G. In the upper part, there are calcitic ashes with a high content of silica phytoliths and calcined bone remains, all denoting high-intensity combustion (Bergadà, 1998; Villagran et al., 2017), but probably below 750–850°C, as the phytoliths do not show signs of melting (Canti, 2003). This hearth appears with the freeze and thaw traces typical of Unit H. It also subsequently underwent dissolution and reprecipitation processes, forming microsparitic to sparitic $CaCO_3$ infillings in the ashes as well as in the fissures of the bones, which, in some cases, led to their fragmentation. Its formation is due to local dissolution of ashes, followed by precipitation. Slow crystallization is evidenced by crystal sizes of >50 µm, indicating a very cool environment and stable conditions (Durand et al., 2010).

In all, the microstratigraphic study shows that there are practically no differences between the hearths analyzed, despite their time difference. These combustions reached high temperatures, which is probably why there are practically no charcoal fragments. It is difficult to hypothesize the function of these hearths as there is a lack of micro-scale studies on the extent of these combustion areas.

Finally, the good preservation of the ashes, with no evidence of dispersion especially in the hearths of Units C and H, could indicate a lack of reiterated occupations in the rockshelter. However, these considerations must be interpreted with caution, as very few hearths have been analyzed from a microstratigraphic point of view at this site.

5.2.2 | Unit G (AL IV)

This unit is associated with a high density of anthropogenic and biogenic components that distinguish it from the rest of the record. Two of the most important are bones and teeth, some with traces of thermoalteration and to a lesser extent fat-derived char.

Some bones have in situ breakage that resulted in articulated and slightly displaced fragments, most likely due to trampling (Miller et al., 2009; Villagran et al., 2017). These data reinforce evidence for human activity in the unit that, in some cases, is related to combustion. One of the aspects worth highlighting about these components is their diagenetic evolution according to the localized MU. In the silty clay MU.22 and MU.24 with high organic contents, bone remains are more abundant. The bone remains are generally reddish-brown, and in some cases, have stains that appear reddish-orange in PPL. These features are due to microbial activity leading to the precipitation of iron and manganese compounds (Bergadà et al., 2013; Polo-Díaz & Fernández-Eraso, 2010; Villagran et al., 2017) and also due to the precipitation of humic acids from the soil (Villagran et al., 2017). This would accentuate the dissolution features, giving rise to an increase in porosity and more subrounded contours at the bone edges due to the acidic environment (Karkanas & Goldberg, 2019). Other bone fragments have calcified filament infillings of fungal origin (Durand et al., 2010).

In contrast, in the $CaCO_3$ silty clay MU.21 and MU.23, microbial activity in the bone fragments is considerably reduced, which is also

an indication that carbonate precipitation was rapid, immediately after the formation of the MU. One of the features affecting bone remains is their enrichment in carbonate in their pores or at their edges, which, in some cases, causes their fragmentation. This process is due to carbonate-rich solutions derived from the surroundings reacting with the phosphate material in the bones. It is these MU that we believe best preserve the hearths such as the one located in grid square G-3 discussed in the previous section, since cementation prevents the proliferation of biological activity in the soil.

The components of plant origin are both uncharred and charred. Some are woody and associated with calcium oxalate crystals, and their presence may be due to combustion taking place at a low temperature (Milek, 2014) or due to poor oxidizing conditions (Courty et al., 1989), data that, when associated with the main traces of thermoalteration observed in some bones, also reflect moderate temperatures. A smaller proportion of woody ash remains are reworked mainly by biological activity.

It is worth mentioning that some coprolites of animals with carnivorous and herbivorous diets have been found in different MU but penecontemporaneous to Neanderthal activity. All these features, as well as the pedogenic activity that developed, allow us to infer that the rate of sedimentation was slow, diffuse, and irregular, and therefore, the occupation surfaces were subaerially exposed, favoring the formation of cumulative palimpsests (Bailey, 2007).

In this unit, occupations were more recurrent in the settlement, but at the same time intermittent and/or seasonal, as there are also features that indicate that it was frequented by animals.

5.3 | Chronostratigraphic and paleoenvironmental evolution

Some challenges arise in establishing the chronostratigraphic and paleoenvironmental evolution of the site (Table 4) in its regional context, because from a chronological point of view, it only has a series of dates that cover the part from Unit E (AL VI) to Unit H (AL III). The dates obtained from Unit E *c.*80.0–83.2 ka give us a reference *ante quem* of the lower part of the sequence and allow us to make some conjectures.

The first episode, Unit A (AL IX), was part of the bed or bar of the ephemeral stream. It is difficult to infer its attribution on a temporal and especially isotopic scale. It can be correlated by the ~8–10 m height of the deposit to other terraces that have been estimated to correspond to the Late Pleistocene. These terraces include the Tuéjar river terrace, T5 of 10–15 m (Martínez-Gallego, 1987), which is part of the drainage basin of the Rambla de Ahíllas and the lower Turia, level III of 5–10 m (Carmona, 1982; Pérez-Cueva, 1985).

According to the available data, this unit corresponds to a torrential flood under arid climatic conditions with a decrease in vegetation cover and an increase in erosion and consequently an increase in sediment production. It is suggested that aggradation probably occurred during the cold stadials of MIS 5. A period of aggradation of the fluvial systems in the Iberian Range and in other Mediterranean localities has been identified during stadial 5d (Soria-Jáuregui et al., 2016), perhaps also the case of Abrigo de la Quebrada.

Subsequently, calcium carbonate cementation processes occurred, giving rise to a petrocalcic horizon, which is a common advanced-phase calcic horizon in Pleistocene alluvial records from Iberia (López-Campuzano et al., 2007; Roquero et al., 1999), usually found in arid or semi-arid environments (Soil Survey Staff, 2015).

After a sedimentary interruption, Unit B (AL VIIIc and b) was formed by debris contributions, as well as by episodes of alluvium from the ephemeral stream. The energy is less in these episodes relative to those before. The layout of the deposit suggests that the rockshelter was not part of the main channel of the ephemeral stream. This is an episode, unlike the previous one, where more evidence of human activity is found.

This is followed by Unit C (AL VIIIa). As we have pointed out in the previous section, its formation and evolution are complex, as several processes are involved. First, cold environmental conditions led to frost-shattering processes that produce abundant clasts, some of large size, as well as some collapse of the rockshelter roof, resulting in a change in the morphology of the site. Then, as the topography of the basal units shows a slight slope, there were certain displacements caused by the effects of thawing and solifluction processes, and it is in this episode that we locate the Neanderthal occupations in the rockshelter. From an environmental point of view, conditions have eased and in some areas of the rockshelter, even calcretes are produced by the biological activity of cyanobacteria. By way of correlation, perhaps this last environmental episode could already be linked to a more benign interstadial period of MIS 5.

Next, there is an episode of stability and biostasis that led to a significant growth of carbonate concretions in the rockshelter roof; this would be in line with the wetter and probably more temperate conditions of the interstadial period, which could be correlated with the tuffaceous records located in the Iberian Range, especially those recorded in the valley of the Ebrón river, a tributary of the Turia river dated between MIS 6–MIS 5180–100 ka (Sancho et al., 2015), or it is also correlated with the formation of speleothems in the northernmost part of the Iberian Range such as the Grutas del Cristal (Teruel, Spain), in which the greatest growth of these formations would occur between 110 and 100 ka related to MIS 5c, a warm period (Moreno et al., 2013). After this episode of stability and biostasis, Unit D (AL VII) formed, characterized by a second collapse from the roof that led to a change in the morphology of the rockshelter and caused a mass displacement of the detrital material. Then, sedimentary deposition slowed based on evidence of increased biological activity, particularly plant roots and a proliferation of gastropods, in an environment with a tendency to ambient humidity. Human activity decreases in relation to the previous unit.

From there, and especially in the sectors furthest from the rockshelter wall, there are different alluvial accumulations from the Rambla de Ahíllas, Unit E (AL VI). Higher energy marks the initial episodes with erosional contact present, although there is a dominance of fine-grained particles and little presence of cobbles. The localized MU indicate that this phase of aggradation was

TABLE 4 Synthesis of the Late Pleistocene evolution of the Abrigo de la Quebrada.

Unit	Archaeological level	Pedosedimentary and anthropic processes	Palaeoenvironment	Dates	MIS Age
A	IX	Alluvial: bar/channel bottom. $CaCO_3$ accumulation -petrocalcic horizon. No human occupation	Arid, decreased vegetation cover		MIS 5 (d?)
B	VIIIb/VIIIc	Local debris and Alluvial episode. (Less) $CaCO_3$ accumulation	(Less) arid		MIS 5
C	VIIIa	Gelifraction, overhang roof collapse and solifluxion. Laminar crusts - calcrete. Human occupation (combustion features)	Cold (arid to humid)		MIS 5
		Short biostasy - episode of growth of carbonate precipitation on the roof of the rockshelter (in form of speleothem)	Humid and warm		MIS 5
D	VII	Overhang roof collapse, mass displacement/pedogenesis	Temperate (arid to humid)		MIS 5
E	VI	Alluvial (granodecrescent sequence). MU.5 and MU.6- flash flood. MU.7-MU.14. - low energy, receding waters. MU.15-MU.18.- floodplain. No human occupation	Temperate and increased rainfall. Increased vegetation cover	80.0 ± 4.7 ka 83.2 ± 5.4 ka	MIS 5a
		Erosion, incision Rambla de Ahíllas			Boundary MIS 5 - MIS 4
F	V	Muddy flow and the beginnings of pedogenesis	Temperate (to more arid conditions)	> 47.1k 14C a BP	MIS 4 or MIS 4/3
G	IV	Diffuse runoff (rainfall). Pedogenesis - organic horizon-, biostatic stage. Important human occupation (combustion features)	Temperate (to humid conditions)	43.9 ± 0.7k 14C a BP >51.6k 14C a BP	
H	III-II	Cryogenesis and gelifluction. Human occupation (combustion features)	Cold (to humid conditions)	40.5 ± 0.5k 14C a BP (III) >50.8k 14C a BP (III)	MIS 4/3

Note: The dashed lines show proposed episodes not recorded in the sedimentary fill. The MIS age have been based on LR04 stack of marine benthic foraminiferal δ18O data (Railsback et al., 2015).

Abbreviation: MU, microunit.

characterized by flooding events that resulted in the deposition of fine material from reduced flow velocities typical of a vegetation covered area. The top of the Unit E functions as a floodplain with certain stability in the environment. The resulting conditions would be temperate and with higher rainfall. This episode would be dated between 80.0 ± 4.7 and 83.2 ± 5.4 ka, which would place it chronostratigraphically around MIS 5a. At Cueva Antón in the Mula Valley (Murcia, Spain), an alluvial accumulation episode is also situated in MIS 5a and characterized by a warm climate and high rainfall (Angelucci et al., 2018).

After Unit E, we propose an incision phase of the Rambla de Ahíllas, since after this episode, no fluvial accumulations are found in the rockshelter. In some basins of the SE peninsular, a phase of river incision has been attributed to the beginning of MIS 4 in the case of the Aguas River in Almería (Shulte, 2002) and to the MIS 4 itself in the Mula Valley, Cueva Antón (Angelucci et al., 2018). Soria-Jáuregui et al. (2016) proposed for the upper River Ebro (northern Iberian Peninsula) that river incision would occur in phases of climatic transition from glacial to interglacial conditions and vice versa. Based on all these data, we speculate as a hypothesis that this episode was chronostratigraphically located in the transition from MIS 5 to MIS 4.

After a period of sedimentary interruption in the Abrigo de la Quebrada, Units F (AL V) and G (AL IV) accumulate, which stand out for their pedogenetic evolution with a redistribution of carbonates and an amorphous organic accumulation of vegetal origin that is mixed with the remains of human activity, mainly in Unit G. The environmental conditions would have been temperate, with periods of oscillating humidity. This is indicative of environmental stability typical of a biostasis phase. The dates obtained place these units at around 43.9k 14C a B.P. and >51.6k 14C a B.P., which, although not precise, are chronostratigraphically located in MIS 4 or MIS 4/3. In the upper Turia basin, specifically in Gestalgar, 45 km from the site, in a deposit corresponding to an alluvial fan that crowns the T1 terrace of the valley, an illuvial clay horizon (Bt) is located in level II, dated by

thermoluminescence at 45 and 46 ka and attributed to MIS 3 (Fumanal, 1996). This indicates that around this time, there were phases of stability that allowed the development of soils in the Pleistocene records. To all this, we must add that in Unit G, there are bone remains of the Mediterranean tortoise (*Testuto hermanni*). There are also some indications of their presence in MIS 4/3, although they were mostly present in the Iberian Peninsula during the Last Interglacial (Morales Pérez & Serra, 2009; Real et al., 2021).

From Unit G onwards, an erosional contact is observed in some sectors and the environmental conditions worsen considerably, as determined in Unit H, dated at 40.5k 14C a B.P. and >50.8k 14C a B.P. (AL III). There are episodes of frost shattered clasts and gelifluction that would be associated with cold oscillations. The dating, as in Unit G, does not offer a good resolution; however, it could also be placed in MIS 4/3. In any case, in the absence of a set of dates, we believe that the inferred paleoenvironmental data are insufficient to make any chronostratigraphic approximation for Units G and H. We are further limited by few specific records for MIS 4 in Iberia that can offer a view of this period (Mallol et al., 2019). It should also be added that the geoarchaeological study carried out at the nearby Abric del Pastor (Alcoi, Spain), located in MIS 4 and the beginning of MIS 3, does not reflect any paleoenvironmental differences either, with evidence of generally cold conditions (Mallol et al., 2019). In any case, what we can suggest is that these units correspond to contrasting paleoenvironmental conditions: Unit G (AL IV) corresponding to a more temperate, interstadial phase and Unit H (AL III-II) corresponding to a colder, stadial phase. These units may perhaps already be located at the beginning of MIS 3, as characterized in different proxies by rapid climatic changes (D'Errico & Sánchez-Goñi, 2003) and reflected in different chronostratigraphic proposals of this isotopic stage (Railsback et al., 2015; Rasmunssen et al., 2014).

6 | CONCLUSIONS

The stratigraphic sequence offered by the Abrigo de la Quebrada represents an excellent record of the beginning of the Late Pleistocene in the upper basin of the River Turia in the Iberian Range. For this reason, Abrigo de la Quebrada, apart from contributing to the archaeological knowledge of the Neanderthal occupations in this area, also becomes an indispensable witness from the geoarchaeological and geomorphological points of view of the evolution of the Rambla de Ahíllas ravine and, in short, of the Turia river.

A relevant aspect of the Rambla de Ahíllas ravine evolution is the incision of the ephemeral stream, between Unit E (AL VI) and F (AL V). This in fact preserved the site from later erosive actions and contributed, from our point of view, to the fact that human occupations were more recurrent at the site, since it would have made the ravine a much more accessible route.

The site can be described as an alluvial terrace in which a water flow dynamic has been detected, with intermittent floods alternating with debris from around the rockshelter. In addition to these processes, the retreat of the rockshelter roof along the sequence favored postdepositional dynamics and soil formation. It is during these biostasis phases, with a tendency toward stability, that human occupations increase, while at the same time, they have a palimpsestic nature due to the slow burial of the surfaces of the occupation, as is the case of Unit G (AL IV). In some MU of this same unit, the formation of carbonate laminae has preserved anthropogenic features in the sedimentary fill.

Discontinuities are reflected throughout the stratigraphic record. There is a more contrasting paleoenvironmental variability from a microstratigraphic point of view in the upper units (Units F, G and H)—MIS 4/3—especially in the more temperate Unit G (AL IV) and in the cooler Unit H (AL III and II). On the other hand, the lower units (from Unit A to Unit E)—MIS 5—are generally temperate, except for Unit C (AL VIIIa), where there is evidence of cold. However, the phases of most active morphogenesis are located in the lower units of the record. These phases of active morphogenesis are more closely related to the alluvial dynamics of the ephemeral stream.

In short, we believe that a geoarchaeological and microstratigraphic vision can be another tool to understand the interaction of geogenic and anthropogenic processes at the site and can provide not only the evolutionary history of the sedimentary record but also of its immediate surroundings, contributing to more detailed knowledge of the *modus vivendi* of the Neanderthal communities that inhabited the Ahíllas ravine.

AUTHOR CONTRIBUTIONS

M. Mercè Bergadà: Conceptualization; methodology; investigation; formal analysis; writing—original draft; writing—review and editing. **Aleix Eixea**: Investigation; funding acquisition; writing—original draft; writing—review and editing; project administration. **Valentín Villaverde**: Investigation; funding acquisition; writing—original draft; writing—review and editing; project administration.

ACKNOWLEDGMENTS

The authors would like to thank Josep M. Cervelló, geologist and member of the Institut d'Arqueologia de la Universitat de Barcelona (IAUB), for his comments regarding the carbonate concretions located in Unit D (AL VII). This research formed part of three projects: *El pasado lejano: aproximación a la conducta y la ocupación del territorio en el paleolítico valenciano* (the distant past: an approach to the behavior and occupation of the territory in the Valencian Palaeolithic period) (PROMETEO/2017/060); *Síntesis del Paleolítico medio y superior en Valencia y Murcia: aspectos cronológicos, paleoambientales, económicos y culturales* (synthesis of the middle and upper palaeolithic in Valencia and Murcia: chronological, paleoenvironmental, economic and cultural aspects) (HAR2017-85153-P); and finally, project PID2021-122308NA-I00 funded by MCIN/AEI/10.13039/501100011033/and by FEDER A way of doing Europe. The authors thank the reviewers and editors for their comments, recommendations, and corrections.

ORCID

M. Mercè Bergadà http://orcid.org/0000-0003-3637-7793
Aleix Eixea http://orcid.org/0000-0002-6228-4294
Valentín Villaverde https://orcid.org/0000-0002-2876-0306

REFERENCES

Alonso-Zarza, A. M., & Wright, V. P. (2010). Calcretes. In A. M. Alonso-Zarza & L. H. Tanner (Eds.), *Carbonates in continental settings: Facies, Environments, and Processes. Developments in sedimentology* (Vol. 61, pp. 226–267). Elsevier.

Angelucci, D. E., Anesin, D., Susini, D., Villaverde, V., Zapata, J., & Zilhão, J. (2018). A tale of two gorges: Late quaternary site formation and surface dynamics in the Mula basin (Murcia, Spain). *Quaternary International*, *485*, 4–22.

Assens, J., Ramírez del Pozo, J., & Giannini, J. (1973). *Mapa geológico y Memoria de la Hoja n° 666 (Chelva). Mapa Geológico de España E. 1:50.000. Segunda Serie* (Primera edición). IGME.

Badal, E., Villaverde, V., & Zilhão, J. (2012). Middle Paleolithic wood charcoal from three Southern Iberian sites: Biogeographic implications. Wood and charcoal. Evidence for human and natural history. *Saguntum Extra*, *13*, 13–24.

Bailey, G. (2007). Time perspectives, palimpsests and the archaeology of time. *Journal of Anthropological Archaeology*, *26*, 198–223.

Bergadà, M. M. (1998). *Estudio geoarqueológico de los asentamientos prehistóricos del Pleistoceno Superior y el Holoceno inicial en Catalunya*. Archaeopress.

Bergadà, M. M., Villaverde, V., & Román, D. (2013). Microstratigraphy of the Magdalenian sequence at Cendres Cave (Teulada-Moraira, Alicante, Spain): Formation and diagenesis. *Quaternary International*, *315*, 56–75.

Bertran, P., & Texier, J. P. (1999). Facies and microfacies of slope deposits. *Catena*, *35*, 99–121.

Boixadera, J., & Poch, R. M. (2008). *Transcatalonia N-S. Guía de excursión de edafología*. Departament de Medi Ambient i Ciències del Sòl (UdL). Lleida: Secció d'Avaluació de Recursos Agraris (Generalitat de Catalunya).

Brochier, J. E. (1996). Feullies ou fumiers? Observations sur le rôle des opusieres sphérolitiques dans l'interprétation des dépôts archéologiques holocènes. *Anthropozoologica*, *24*, 19–30.

Brönnimann, D., Ismail-Meyer, K., Rentzel, P., Pümpin, C., & Lisá, L. (2017). Excrements of herbivores. In C. Nicosia & G. Stopps (Eds.), *Archaeological soil and sediment micromorphology* (pp. 55–65). Blackwell Science Ltd.

Brönnimann, D., Pümpin, C., Ismail-Meyer, K., Rentzel, P., & Égüez, N. (2017). Excrements of omnivores and carnivores. In C. Nicosia & G. Stoops (Eds.), *Archaeological soil and sediment micromorphology* (pp. 67–81). Blackwell Science Ltd.

Bullock, P., Fedoroff, N., Jongerius, A., Stoops, G., & Tursina, T. (1985). *Handbook for soil thin section description*. Waine Research Publications.

Canti, M. G. (2003). Aspects of the chemical and microscopic characteristics of plant ashes found in archaeological soils. *Catena*, *54*, 339–361.

Canti, M. G. (2017). Biospheroids produced by earthworms. In C. Nicosia & G. Stoops (Eds.), *Archaeological soil and sediment micromorphology* (pp. 47–49). Blackwell Science Ltd.

Carbonell, E., Huguet, R., Cáceres, I., Lorenzo, C., Mosquera, M., Ollé, A., Rodríguez, X. P., Saladié, P., Vergés, J. M., García-Medrano, P., Rosell, J., Vallverdú, J., Carretero, J. M., Navazo, M., Ortega, A. I., Martinón-Torres, M., Morales, J. I., Allué, E., Aramburu, A., … & Arsuaga, J. L. (2014). Los yacimientos arqueológicos de la Sierra de Atapuerca. In R. Sala (Ed.), *Los cazadores recolectores del Pleistoceno y del Holoceno en Iberia y el estrecho de Gibraltar:estado del conocimiento del registro arqueológico* (pp. 534–560). Universidad de Burgos, Fundación de Atapuerca.

Carmona, P. (1982). Las terrazas del bajo Turia. *Cuadernos de Geografía*, *30*, 41–62.

Carrión-Marco, Y., Guillem Calatayud, P., Eixea, A., Martínez-Varea, C. M., Tormo, C., Badal, E., Zilhão, J., & Villaverde, V. (2019). Climate, environment and human behaviour in the Middle Palaeolithic of Abrigo de la Quebrada (Valencia, Spain): The evidence from charred plant and micromammal remains. *Quaternary Science Reviews*, *217*, 152–168. https://doi.org/10.1016/j.quascirev.2018.11.032

Connolly, R., Jambrina-Enríquez, M., Herrera-Herrera, A. V., Vidal-Matutano, P., Fagoaga, A., Marquina-Blasco, R., Marin-Monfort, M. D., Ruiz-Sánchez, F. J., Laplana, C., Bailon, S., Pérez, L., Leierer, L., Hernández, C. M., Galván, B., & Mallol, C. (2019). A multiproxy record of palaeoenvironmental conditions at the Middle Palaeolithic site of Abric del Pastor (Eastern Iberia). *Quaternary Science Reviews*, *225*, 106023.

Courty, M. A., Goldberg, P., & Macphail, R. I. (1989). *Soils and micromorphology in archaeology*. University Press.

D'Errico, F., & Sánchez Goñi, F. (2003). Neandertal extinction and the millennial scale climatic variability of OIS 3. *Quaternary Science Reviews*, *22*, 769–788.

Doménech, E. M. (2005). La transición del Paleolítico medio al superior en la Cova Beneito (Muro, Alicante): Recientes aportaciones. In A. Pérez-González, M. Santonja, & M. J. Machado (Eds.), *Geoarqueología y patrimonio en la Península Ibérica y el entorno mediterráneo* (pp. 197–203). ADEMA.

Domingo, R., Peña-Monné, J. L., de Torres, T., Ortiz, J. E., & Utrilla, P. (2017). Neanderthal highlanders: Las Callejuelas (Monteagudo del Castillo, Teruel, Spain), a high-altitude site occupied during MIS 5. *Quaternary International*, *435*, 129–143.

Dorronsoro, F., Stoops, G., Aguilar, J., Dorronsoro-Diaz, C., Fernández, J., Diez, M., & Dorronsoro, B. (2020). Carbonatos en suelos. Programa sobre el proceso de acumulación y lavado de los carbonatos y de los rasgos resultantes de su actuación en los suelos. In F. Dorronsoro (Ed.), *Libros web, monografías, trabajos de investigación, conferencias, atlas sobre la Edafología y los suelos*. Departamento de Edafología y Química Agrícola, Universidad de Granada. https://edafologia.ugr.es/carbonat/index.htm

Ducloux, J., & Laouina, A. (1989). The pendent calcretes in semi-arid climates: An example located near Taforalt, NW Morocco. *Catena*, *16*(3), 237–249.

Durand, N., Monger, C. H., & Canti, M. G. (2010). Calcium carbonate features. In G. Stoops, V. Y. Marcelino, & F. Mees (Eds.), *Interpretation of micromorphological features of soils and regoliths* (pp. 149–194). Elsevier.

Eixea, A., Chacón, M. A., Bargalló, A., Sanchis, A., Romagnoli, F., Vaquero, M., & Villaverde, V. (2020). Neanderthal spatial patterns and occupation dynamics: A focus on the central region in Mediterranean Iberia. *Journal of World Prehistory*, *33*, 267–324.

Eixea, A., Oltra, I., Bergadà, M. M., & Villaverde, V. (2020). The reinterpretation of the Cova Negra archaeological and stratigraphical sequence and its implications in the understanding of the Middle Palaeolithic Iberian Peninsula. *Quaternary International*, *566–567*, 98–112.

Eixea, A., Villaverde, V., & Zilhão, J. (2011). Aproximación al aprovisionamiento de materias primas líticas en el yacimiento del Paleolítico medio del Abrigo de la Quebrada (Chelva, Valencia). *Trabajos de Prehistoria*, *68*(1), 65–78.

Eixea, A., Villaverde, V., Zilhão, J., Sanchis, A., Morales, J. V., Real, C., & Bergadà, M. M. (2011–2012). El nivel IV del abrigo de la quebrada (Chelva, Valencia). Análisis microespacial y valoración del uso del espacio en los yacimientos del Paleolítico medio valenciano. *Mainaké*, *XXXIII*, 131–162.

Esteban, I., Albert, R. M., Eixea, A., Zilhão, J., & Villaverde, V. (2017). Neanderthal use of plants and past vegetation reconstruction at the Middle Paleolithic site of Abrigo de la Quebrada (Chelva, Valencia, Spain). *Archaeological and Anthropological Sciences*, *9*, 265–278.

Fernández-Peris, J. (2007). *La Cova del Bolomor (Tavernes de la Valldigna, Valencia). Las industrias del Pleistoceno Medio en el ámbito del Mediterráneo Peninsular* (Servicio de Investigación Prehistórica, 108). Valencia: Diputación provincial de Valencia.

Fernández-Peris, J., & Martínez-Valle, R. (1989). El yacimiento del Paleolítico medio de San Luis (Buñol, Valencia). *Saguntum*, *22*, 11–34.

Fumanal, M. P. (1996). Aspectos paleoambientales del País Valenciano. *Notes de Geografia física*, *25*, 41–65.

Galván, B., Hernández, C. M., Mallol, C., Mercier, N., Sistiaga, A., & Soler, V. (2014). New evidence of early Neanderthal disappearance in the Iberian Peninsula. *Journal of Human Evolution*, *75*, 16–27.

Ismail-Meyer, K. (2017). Plant remains. In C. Nicosia & G. Stoops (Eds.), *Archaeological soil and sediment micromorphology* (pp. 121–135). Blackwell Science Ltd.

Karkanas, P., & Goldberg, P. (2013). Micromorphology of cave sediments. In J. F. Shroder & A. Frumkin (Eds.), *Treatise on geomorphology* (Vol. 6, pp. 286–297). Academic Press.

Karkanas, P., & Goldberg, P. (2019). *Reconstructing archaeological sites understanding the geoarchaeological matrix*. Wiley-Blackwell.

López-Campuzano, M., & Conesa, C. (2008). Yacimientos del Paleolítico Medio de las Rambla del Rincón, Cañizares y Tobarrillas (Yecla, Múrcia). Estudio comparativo de estratigrafía aluvial. *Memorias de Arqueología de la región de Múrcia*, *15*, 107–128.

López-Campuzano, M., Conesa, C., & Marín, J. A. (2007). El yacimiento de Paleolítico Medio de la Rambla del Rincón (Yecla, Múrcia). Estudio estratigráfico y sedimentológico. *Verdolay*, *10*, 13–39.

Mallol, C., Hernández, C., Mercier, N., Falguères, C., Carrancho, Á., Cabanes, D., Vidal-Matutano, P., Connolly, R., Pérez, L., Mayor, A., Ben Arous, E., & Galván, B. (2019). Fire and brief human occupations in Iberia during MIS 4: Evidence from Abric del Pastor (Alcoy, Spain). *Scientific Reports*, *9*, 18281. https://doi.org/10.1038/s41598-019-54305-9

Mallol, C., Mentzer, S. M., & Miller, C. E. (2017). Combustion features. In C. Nicosia & G. Stoops (Eds.), *Archaeological soil and sediment micromorphology* (pp. 299–330). Blackwell Science Ltd.

Martínez-Gallego, J. (1987). Geomorfología de los depósitos cuaternarios de Chelva (Valencia). *Mediterránea Serie de Estudios Geológicos*, *6*, 131–138.

Mateo, J. F., Burguet, I., Fábrega, C., Nebot, J., Pardo, J., & Viñals, M. J. (1988). Geomorfología y colonización vegetal en ramblas de zonas calcáreas: El Saltador de la Rambla de la Viuda. *Cuadernos de Geografía*, *44*, 145–162.

Mazo, C., & Alcolea, M. (2020). New data concerning Neanderthal occupation in the Iberian System: First results from the Late Pleistocene (MIS 3) Aguilón P5 cave site (NE Iberia). *Quaternary International*, *551*, 105–122.

Mentzer, S. M. (2014). Microarchaeological approaches to the identification and interpretation of combustion features in prehistoric archaeological sites. *Journal of Archaeological Method and Theory*, *21*(3), 616–668.

Milek, K. B. (2014). Micromorphology of occupation deposits on archaeological sites. In L. Lisá (Ed.), *Soil micromorphology in general and archaeological context* (pp. 60–79). Mendel University in Brno.

Miller, C., Conard, N. J., Goldberg, P., & Berna, F. (2009). Dumping, sweeping and trampling: Experimental micromorphological analysis of anthropogenically modified combustion features. *Palethnologie*, *2009*, 25–37.

Morales Pérez, J. V., & Serra, A. S. (2009). The quaternary fossil record of the genus Testudo in the Iberian Peninsula. Archaeological implications and diachronic distribution in the western Mediterranean. *Journal of Archaeological Science*, *36*, 1152–1162.

Moreno, A., Belmonte, A., Bartolomé, M., Sancho, C., Oliva, B., Stoll, H., Edwards, L. R., Cheng, H., & Hellstrom, J. (2013). Formación de espeleotemas en el noreste peninsular y su relación con las condiciones climáticas durante los últimos ciclos glaciares. *Cuadernos de Investigación Geográfica*, *39*(1), 25–47.

Nicosia, C., & Stoops, G. (2017). *Archaeological soil and sediment micromorphology*. Blackwell Science Ltd.

Pérez-Cueva, A. J. (1985). *Geomorfología del sector oriental de la Cordillera Ibérica entre los ríos Migares y Turia* [Tesis doctoral, Universidad de Valencia].

Polo-Díaz, A., & Fernández-Eraso, J. (2010). Same anthropogenic activity, different taphonomic processes: A comparison of deposits from Los Husos I & II (Upper Ebro Basin, Spain). *Quaternary International*, *214*(1–2), 82–97.

Railsback, L. B., Gibbard, P. L., Head, M. J., Voarintsoa, N. R. G., & Toucanne, S. (2015). An optimized scheme of lettered marine isotope substages for the last 1.0 million years, and the climatostratigraphic nature of isotope stages and substages. *Quaternary Science Reviews*, *111*, 94–106.

Rasmussen, S. O., Bigler, M., Blockley, S. P., Blunier, T., Buchardt, S. L., Clausen, H. B., Cvijanovic, I., Dahl-Jensen, D., Johnsen, S. J., Fischer, H., Gkinis, V., Guillevic, M., Hoek, W. Z., Lowe, J. J., Pedro, J. B., Popp, T., Seierstad, I. K., Steffensen, J. P., Svensson, A. M., … Winstrup, M. (2014). A stratigraphic framework for abrupt climatic changes during the Last Glacial period based on three synchronized Greenland ice-core records: Refining and extending the INTIMATE event stratigraphy. *Quaternary Science Reviews*, *106*, 14–28.

Real, C., Eixea, A., Sanchis, A., Morales, J. V., Klasen, N., Zilhão, J., & Villaverde, V. (2020). Abrigo de la Quebrada Level IV (Valencia, Spain): Interpreting a middle palaeolithic palimpsest from a zooarchaeological and lithic perspective. *Journal of Paleolithic Archaeology*, *3*, 187–224. https://doi.org/10.1007/s41982-018-0012-z

Real, C., Martínez-Varea, C. M., Carrión, Y., Badal, E., Sanchis, A., Guillem, P., Martínez-valle, R., & Villaverde, V. (2021). Could the central-eastern Iberian Mediterranean region be defined as a refugium? Fauna and flora in MIS 5-3 and their implications for Palaeolithic human behaviour. *Journal of Quaternary Science*, *37*, 363–379. https://doi.org/10.1002/jqs.3285

Real, C., Sanchis, A., Eixea, A., Zilhão, J., & Villaverde, V. (2019). Cambios en los modeloseconómico y de ocupación del abrigo de la Quebrada (Chelva, Valencia). Nuevosdatos arqueozoológicos y tafonómicos del nivel VII (MIS 5). *Recursos marins en el passat. IV Jornadesd'arqueozoologia* (pp. 257–277). Museu de Prehistòria de València.

Rios-Garaizar, J., & Eixea, A. (2021). Lithic technological choices of Late Neandertals in a mountain environment south of the Ebro Valley, Iberian Peninsula (Peña Miel level e). *Archaeological and Anthropological Sciences*, *13*, 123. https://doi.org/10.1007/s12520-021-01360-x

Roquero, E., Goy, J. L., & Zazo, C. (1999). Fenómenos de convergencia genética en suelos de terrazas fluviales: Valle del río Tajo, Madrid-Toledo, España. *Revista de la Sociedad Geológica de España*, *12*(3–4), 329–338.

Sancho, C., Arenas, C., Vázquez-Urbez, M., Pardo, G., Lozano, M. V., Peña-Monné, J. L., Hellstrom, J., Ortiz, J. E., Osácar, M. C., Auqué, L., & Torres, T. (2015). Climatic implications of the Quaternary fluvial tufa record in the NE Iberian Peninsula over the last 500 ka. *Quaternary Research*, *84*(3), 398–414. https://doi.org/10.1016/j.yqres.2015.08.003

Santonja, M., Pérez-González, A., Domínguez-Rodrigo, M., Panera, J., Rubio-Jara, S., Sesé, C., Soto, E., Arnold, L. J., Duval, M., Demuro, M., Ortiz, J. E., de Torres, T., Mercier, N., Barba, R., & Yravedra, J. (2014). The Middle Paleolithic site of Cuesta de la Bajada (Teruel, Spain): A perspective on the Acheulean and Middle Paleolithic technocomplexes in Europe. *Journal of Archaeological Science*, *49*, 556–571.

Shulte, L. (2002). *Evolución cuaternaria de la depresión de Vera y de Sorbas oriental (SE-Península Ibérica)*. Publicacions de la Universitat de Barcelona.

Soil Survey Staff. (2015). *Illustrated guide to soil taxonomy, version 2*. U.S. Department of Agriculture, Natural Resources Conservation Service. Lincoln Nebraska: National Soil Survey Center.

Soria-Jáuregui, Á., González-Amuchástegui, M. J., Mauz, B., & Lang, A. (2016). Dynamics of Mediterranean late Quaternary fluvial activity: An example from the River Ebro (north Iberian Peninsula). *Geomorphology*, *268*, 110–122.

Stoops, G. (2021). *Guidelines for analysis and description of soil and regolith thin sections* (2nd ed.) Wiley.

Stoops, G., Marcelino, V., & Mees, F. (2010). *Interpretation of micromorphological features of soils and regoliths*. Elsevier.

Utrilla, P., & Álvarez, A. (1985). Excavaciones en la Cueva de los Toros (Cantavieja, Teruel): Campaña de 1984. *Bajo Aragón Prehistoria*, *6*, 9–30.

Utrilla, P., Vilchez, J., Montes, L., Barandiaran, I., Altuna, J., Gil, E., & Lopez, P. (1987). *La cueva de Peña Miel. Nieva de Cameros. La Rioja. Excavaciones Arqueologicas en España 154*. Ministerio de Educacion y Ciencia.

Van Vliet-Lanoë, B. (2010). Frost action. In G. Stoops, V. Marcelino, & F. Mees (Eds.), *Interpretation of micromorphological features of soils and regoliths* (pp. 81–108). Elsevier.

Verrecchia, E. P., Freytet, P., Verrecchia, K. E., & Dumont, J. L. (1995). Spherulites in calcrete laminar crusts: Biogenic $CaCO_3$ precipitation as a major contributor to crust formation. *Journal of Sedimentary Research*, *A65*, 690–700.

Villagran, X. S., Huisman, D. J., Mentzer, S. M., Miller, C. E., & Jans, M. M. (2017). Bone and other skeletal tissues. In G. Stoops & C. Nicosia (Eds.), *Archaeological soil and sediment micromorphology* (pp. 11–38). Blackwell Science Ltd.

Villaverde, V., Eixea, A., & Zilhão, J. (2008). Aproximación a la industria lítica del abrigo de la Quebrada (Chelva, Valencia). *Treballs d'Arqueologia*, *14*, 213–228.

Villaverde, V., Eixea, A., Zilhão, J., Sanchis, A., Real, C., & Bergadà, M. (2017). Diachronic variation in the Middle Paleolithic settlement of Abrigo de la Quebrada (Chelva, Spain). *Quaternary International*, *435*, 164–179.

How to cite this article: Bergadà, M. M., Eixea, A., & Villaverde, V. (2023). Geoarchaeological and microstratigraphic view of a Neanderthal settlement at Rambla de Ahíllas in Iberian Range: Abrigo de la Quebrada (Chelva, Valencia, Spain). *Geoarchaeology*, *38*, 679–712. https://doi.org/10.1002/gea.21973